Tumour-associated macrophages and oncolytic virotherapies

Eftimie, Raluca; Eftimie, G.

Published in:
Letters in Biomathematics

DOI:
10.1080/23737867.2018.1430518

Publication date:
2018

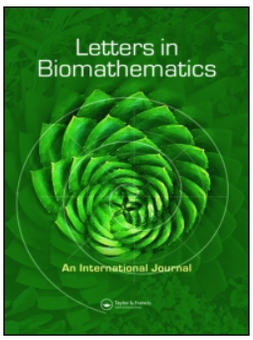

Taylor & Francis
Taylor & Francis Group

Letters in Biomathematics

ISSN: (Print) 2373-7867 (Online) Journal homepage: http://www.tandfonline.com/loi/tlib20

Tumour-associated macrophages and oncolytic virotherapies: a mathematical investigation into a complex dynamics

R. Eftimie & G. Eftimie

To cite this article: R. Eftimie & G. Eftimie (2018) Tumour-associated macrophages and oncolytic virotherapies: a mathematical investigation into a complex dynamics, Letters in Biomathematics, 5:1, 70-99, DOI: 10.1080/23737867.2018.1430518

To link to this article: https://doi.org/10.1080/23737867.2018.1430518

Published online: 06 Feb 2018.

LETTERS IN BIOMATHEMATICS, 2018
VOL. 5, NO. 1, 70–99
https://doi.org/10.1080/23737867.2018.1430518

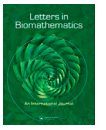

Taylor & Francis
Taylor & Francis Group

RESEARCH ARTICLE

OPEN ACCESS Check for updates

Tumour-associated macrophages and oncolytic virotherapies: a mathematical investigation into a complex dynamics

R. Eftimie[a] and G. Eftimie[b]

[a]Division of Mathematics, University of Dundee, Dundee, UK; [b]Clinique de La Miotte, Belfort, France

ABSTRACT

Anti-cancer therapies based on oncolytic viruses are emerging as important approaches in cancer treatment. However, the effectiveness of these therapies depends significantly on the interactions between the oncolytic viruses and the host immune response. Macrophages are one of the most important cell types in the anti-viral immune responses, by acting as a first line of defence against infections. Here, we consider a mathematical approach to investigate the possible outcomes of the interactions between two extreme phenotypes of macrophages (M1 and M2 cells) and an oncolytic virus (VSV), in the context of B16F10 melanoma. We show that polarization towards either an M1 or M2 phenotype can enhance oncolytic virus therapy through either (i) anti-tumour immune activation, or (ii) enhanced oncolysis. Moreover, we show that tumour reduction and elimination does not depend only on the ratio of M1:M2 cells, but also on the number of tumour-infiltrating macrophages.

ARTICLE HISTORY
Received 22 October 2017
Accepted 16 January 2018

KEYWORDS
Oncolytic viruses; M1 macrophages; M2 macrophages; melanoma cells; mathematical model

1. Introduction

Oncolytic viruses (i.e. viruses that selectively replicate in, and destroy cancer cells) are emerging as an important approach in cancer treatment, due to their potential of inducing systemic anti-tumour immunity in addition to selectively killing cancer cells (Kaufman, Kolhapp, & Zloza, 2016). However, the effectiveness of these viruses – once they are injected into the patient – depends not only on the pathogenic nature of virally encoded genes, but also on the interactions between the virus and the host immune response, which might impact the ability of the virus to replicate (Kaufman et al., 2016).

One of the most versatile types of immune cells, which is also one of the key regulators of cancer immunotherapy, as well as of immunotherapy against exogenous infections, is represented by the macrophages. The macrophages can display different phenotypes, in response to the type, concentration and longevity of exposure to stimulating agents (Cassetta, Cassol, & Poli, 2011). The two extreme macrophages phenotypes are represented by the M1 and M2 cells; see Mantovani, Sozzani, Locati, Allavena, and Sica (2002) and Sica et al. (2008) and also Figure 1. (Note that this M1–M2 classification follows the Th1–Th2

CONTACT R. Eftimie r.a.eftimie@dundee.ac.uk

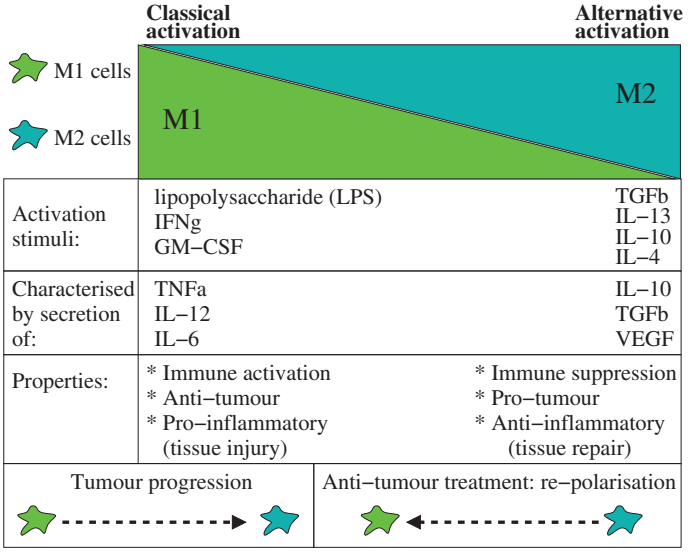

Figure 1. Classification of macrophages phenotypes, where cells are considered as part of a continuum, with the two extreme phenotypes of macrophages polarization being represented by the classically activated M1 cells and the alternatively activated M2 cells.
Notes: Tumour progression induces a M1→M2 polarization (Mantovani and Sica, 2010). Recent studies (Allavena and Mantovani, 2012) have suggested a re-polarization of macrophages towards the M1 anti-tumour phenotype, as a treatment approach to ensure tumour elimination.

$CD4^+$ T cells classification, with the M1 cells being stimulated by Th1 cytokines and the M2 cells being stimulated by Th2 cytokines (Allavena & Mantovani, 2012).) While it is widely accepted that the classically activated M1 cells have anti-tumour properties and the alternatively activated M2 cells have pro-tumour properties, many macrophages inside the tumour microenvironment have markers characterizing mixed phenotypes (Allavena & Mantovani, 2012; Italiani & Boraschi, 2014; Mantovani & Sica, 2010). Therefore, in spite of the fact that macrophages often constitute one of the most common cell types in solid tumours (sometimes forming up to 80% of the total tumour mass; see Jakeman, Hills, Fisher, & Seymour, 2015), their plasticity makes it difficult to fully understand their pro-tumour/anti-tumour roles, as well as their pro-viral/anti-viral roles.

As recently emphasized in Denton, Chen, Scott, and Cripe (2016), the macrophages' role on oncolytic virus therapies is a poorly understood aspect. The M2 macrophages can support these therapies through the suppression of the anti-viral immune response. The M1 macrophages may impede oncolytic therapies through the promotion of an anti-viral immune response that leads to viral clearance, but they also enhance the virus-mediated activation of the anti-tumour immune response (Denton et al., 2016). The complexity of the interactions between macrophages and oncolytic virotherapies depends also on the type of the tumour. It is known, for example, that in the case of glioblastoma oncolytic therapy with Herpex Simplex Virus (HSV), the M1 macrophages hinder this therapy (Meisen et al., 2015) (via the TNFα pathway), while the M2 macrophages promote this therapy (Han et al., 2015) (via the activation of the TFGβ pathway). In contrast, in the case of pancreatic cancer with HSV, the M1 macrophages help this therapy (Liu et al., 2013) (via the activation of the GM-CSF pathway).

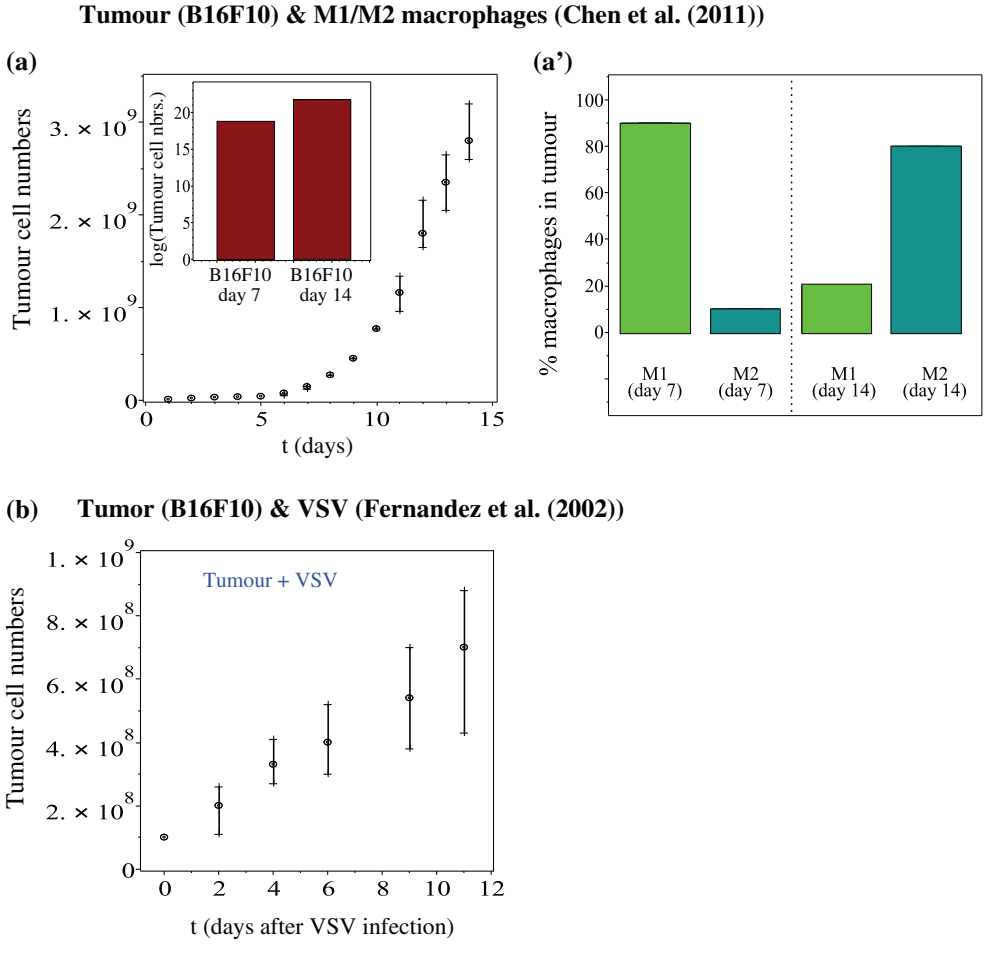

Figure 2. (a) Growth of B16F10 tumour cells and (a') the re-polarization of M1 and M2 macrophages, as described by data re-drawn from Chen et al. (2011). Here, the authors injected mice with 5×10^6 tumour cells. (b) Growth of B16F10 tumour cells in the presence of VSV treatment, as described by data re-drawn from Fernandez et al. (2002). Here, the authors injected mice with 5×10^5 tumour cells, and after palpable tumours were formed (of volumes $\approx$100 mm^3) the mice were treated with 2×10^7 PFU of wild-type VSV.

It is important to emphasize here that also the oncolytic viruses could influence the polarization of tumour-associated macrophages (TAMs) via the induction of tumour-targeted expression of cytokines that can modulate macrophages activation (Jakeman et al., 2015).

In this study, we use a mathematical and computational approach to propose hypotheses that could explain the complex roles of M1 and M2 macrophages during oncolytic viral therapies. Mathematical approaches have been widely used in the past to investigate the interactions between oncolytic viruses, tumour cells and immune cells – mainly cytotoxic T cells; see Nowak and May (2000), Wodarz (2001), Wodarz and Komarova (2009), Friedman et al. (2006), Bajzer, Carr, Josić, Russell, and Dingli (2008), Dingli et al. (2009),

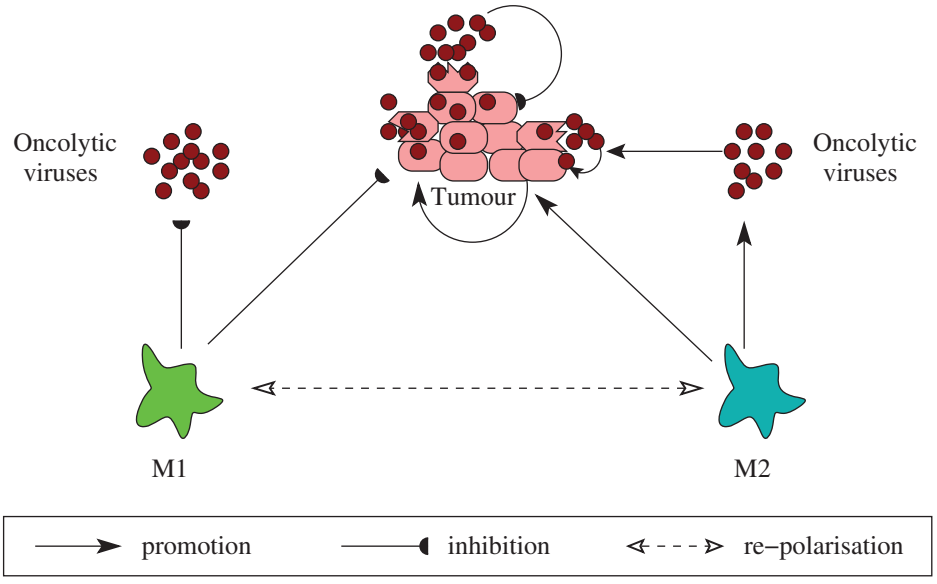

Figure 3. Caricature description of the interactions between the tumour cells, oncolytic viruses and the innate immune responses generated by M1 and M2 macrophages.

Paiva, Binny, Ferreira, and Martins (2009), Komarova and Wodarz (2010), Wu, Kirn, and Wein (2004), Eftimie, Dushoff, Bridle, Bramson, and Earn (2011), Hofacre, Wodarz, Komarova, and Fan (2012), Rommelfanger et al. (2012), Crivelli, Földes, Kim, and Wares (2012), Macnamara and Eftimie (2015), Kim, Crivelli, Choi, Yun, and Wares (2015), Malinzi, Sibanda, and Mambili-Mamboundou (2015), Eftimie, Macnamara, Dushoff, Bramson, and Earn (2016) and the references therein. The majority of these models focus on the temporal evolution of viral titres and immune cell responses (which can be compared with available experimental data), thus, being described by ordinary differential equations. A few mathematical models focus also on the spatial distribution of viruses inside solid tumours (Hofacre et al., 2012; Malinzi et al., 2015; Malinzi, Eladdadi, & Sibanda, 2017; Paiva et al., 2009). Other mathematical models have been derived to investigate the role of M1 and M2 macrophages on tumour dynamics, including B10F16 melanoma (den Breems & Eftimie, 2016; Eftimie & Hamam, 2017; Louzoun, Xue, Lesinski, & Friedman, 2014).

Here, we focus on the B16F10 melanoma (due to availability of some tumour and immune data – see Figure 2 and Section 2.1), and investigate the innate immune responses generated by the M1 and M2 cells during tumour progression. Moreover, we investigate at a theoretical level the effects of M1 and M2 cells on the possible outcomes of oncolytic virus therapies using a Vesicular Stomatitis Virus (VSV). This virus is particularly attractive for viral-based immunotherapies due to its tumour specificity, its rapid replication and its ability to trigger immune responses (Melzer, Lopez-Martinez, & Altomonte, 2017), and as such there is data on the effects of VSV on tumour dynamics; see Figure 2(b). We emphasize that while there are experimental studies that focus on the efficacy of VSV on B16F10 melanoma and the adaptive and innate immune responses, to our knowledge

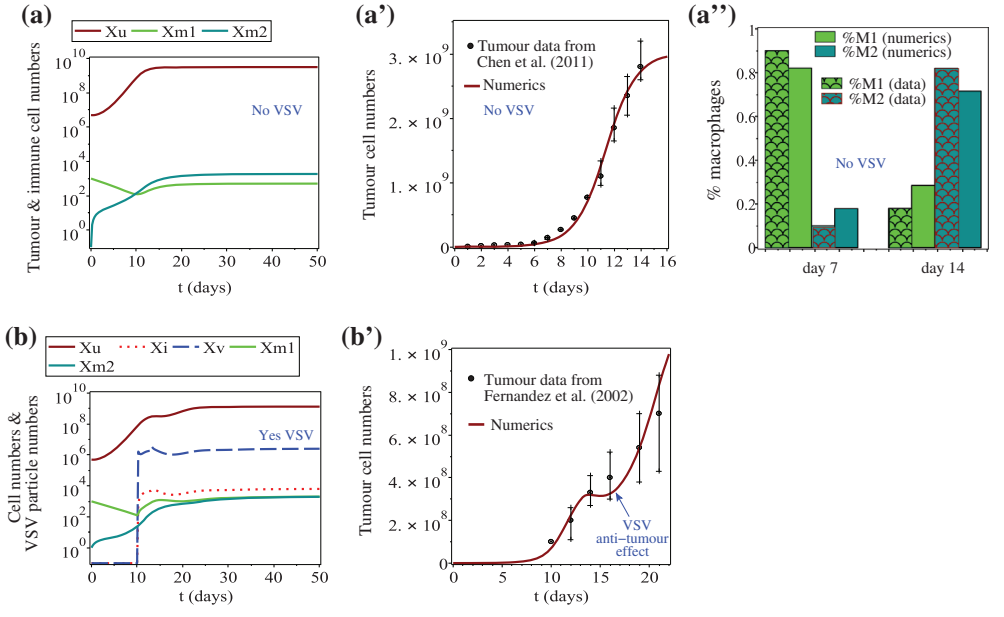

Figure 4. (a)–(a″) Comparison between the numerically simulated dynamics of tumour-M1-M2 cells (in the absence of any VSV treatment) and the experimental data re-drawn from Chen et al. (2011). Initial conditions are $x_u = 5 \times 10^6$, $x_{m1} = 10^3$, $x_{m2} = 1$. (b)–(b′) Comparison between the numerically simulated dynamics of tumour-M1-M2 cells in the presence of VSV treatment and the experimental data re-drawn from Fernandez et al. (2002). Initial conditions are $x_u(0) = 5 \times 10^5$, $x_{m1}(0) = 10^3$, $x_{m2}(0) = 1$, $x_v(0) = x_i(0) = 0$. The injection of 2×10^7 VSV particles on the day ($t = 10$) when tumour reaches $\approx$ 100mm^3, and again 3 days later ($t = 13$), is described by the addition of the following function to the right-hand side of Equation (1c): $H(t) = 2 \times 10^7 \big[\text{Heaviside}(t - 10.1) \times \text{Heaviside}(10.2 - t) + \text{Heaviside}(t - 13.1) \times \text{Heaviside}(13.2 - t)\big]$.
Note: Since the intravenous or intratumoural injection of oncolytic viruses can last from a couple of minutes to a couple of hours (Hotte et al., 2007; Pecora et al., 2002; Kubo et al., 2011), here we model this aspect by assuming that the injection of the VSV particles occurs during 10% of the total daytime, i.e. for $t \in [10.1, 10.2]$ and $t \in [13.1, 13.2]$.

there are no experimental studies that differentiate the effects of M1 and M2 cells on the anti-tumour roles of VSV. To this end, we use a simple ODE model that describes the temporal evolution of cells and virus titres. We first parametrize the model based on different published literature studies. Then we show that tumour elimination could be the result of either the oncolytic therapy or immune therapy. Moreover, we use our model to shed further light on the contradictory results regarding the roles of M1:M2 ratios vs. the numbers of M1 and M2 macrophages inside tumours, on the long-term patient survival (Chen et al., 2011; He et al., 2013; Ma et al., 2010; Ohri, Shikotra, Green, Waller, & Bradding, 2009). We show that in the context of anti-tumour immunity, tumour elimination strongly depends on the total number of tumour-infiltrating macrophages, and not only on the ratio of M1:M2 cells. On the other hand, tumour control depends on the ratio of M1:M2 cells (and not on total number of macrophages). Moreover, in the context of oncolytic therapy, tumour elimination is associated with large numbers of replicating VSV particles, which leads also to large numbers of tumour-infiltrating macrophages.

2. Model description

To investigate the effect of M1 and M2 macrophages on the anti-tumour oncolytic therapy with VSV, we consider a simple mathematical model that describes the time evolution of the following variables: the density of uninfected tumour cells (x_{u}), the density of virus-infected tumour cells (x_{i}), the density of virus particles (x_{v}), the density of M1 macrophages (x_{m1}) and the density of M2 macrophages (x_{m2}); see also Figure 3. The time-evolution of these densities is described by the following equations:

$$\frac{\mathrm{d}x_{\mathrm{u}}}{\mathrm{d}t} = rx_{\mathrm{u}}\left(1-\frac{x_{\mathrm{u}}}{K}\right) - d_v x_{\mathrm{v}}\frac{x_{\mathrm{u}}}{h_u^v + x_{\mathrm{u}}} - d_u x_{\mathrm{u}}\frac{x_{\mathrm{m1}}}{h_m + x_{\mathrm{m2}}} + d_m x_{\mathrm{u}}\frac{x_{\mathrm{m2}}}{h_m + x_{\mathrm{m2}}}, \tag{1a}$$

$$\frac{\mathrm{d}x_{\mathrm{i}}}{\mathrm{d}t} = d_v x_{\mathrm{v}}\frac{x_{\mathrm{u}}}{h_u^v + x_{\mathrm{u}}} - \delta_i x_{\mathrm{i}} - d_i x_{\mathrm{i}}\frac{x_{\mathrm{m1}}}{h_m + x_{\mathrm{m2}}}, \tag{1b}$$

$$\frac{\mathrm{d}x_{\mathrm{v}}}{\mathrm{d}t} = H(t) + \delta_i b x_{\mathrm{i}} - \omega x_{\mathrm{v}} - \delta_v x_{\mathrm{v}}\frac{x_{\mathrm{m1}}}{h_m + x_{\mathrm{m2}}}, \tag{1c}$$

$$\begin{aligned}\frac{\mathrm{d}x_{\mathrm{m1}}}{\mathrm{d}t} &= a_1^v(x_{\mathrm{i}} + x_{\mathrm{v}}) + a_1^u x_{\mathrm{u}} + p_{m_1}x_{m_1}\left(1 - \frac{x_{\mathrm{m1}} + x_{\mathrm{m2}}}{M}\right)\\ &\quad - x_{\mathrm{m1}}\left(r_{m1}^0 + r_{m1}^u\frac{x_{\mathrm{u}}}{h_u + x_{\mathrm{u}}}\right) + x_{\mathrm{m2}}\left(r_{m2}^0 + r_{m2}^v\frac{x_v}{h_v + x_v}\right) - d_e x_{\mathrm{m1}},\end{aligned} \tag{1d}$$

$$\begin{aligned}\frac{\mathrm{d}x_{\mathrm{m2}}}{\mathrm{d}t} &= a_2^u x_u + p_{m_2}x_{m_2}\left(1 - \frac{x_{\mathrm{m1}} + x_{\mathrm{m2}}}{M}\right) + x_{\mathrm{m1}}\left(r_{m1}^0 + r_{m1}^u\frac{x_{\mathrm{u}}}{h_u + x_{\mathrm{u}}}\right)\\ &\quad - x_{\mathrm{m2}}\left(r_{m2}^0 + r_{m2}^v\frac{x_{\mathrm{v}}}{h_v + x_{\mathrm{v}}}\right) - d_e x_{\mathrm{m2}}.\end{aligned} \tag{1e}$$

These equations incorporate the following biological assumptions:

- The uninfected tumour cells proliferate logistically with rate r, up to a carrying capacity K. Note that we use logistic growth because some experimental studies showed evidence of a reduced rate of tumour growth at larger sizes (see e.g. the in vivo and in vitro growth of various human and rodent solid tumours discussed in Laird (1964), Looney, Ritenour, and Hopkins (1980) and Guiot et al. (2003)). We assume that the virus particle infect, at a rate d_v, only a certain proportion of the tumour. This can be modelled using a saturated term for the tumour–virus interactions (with h_u the half saturation constant for tumour cells infected with the oncolytic virus particles). The uninfected tumour cells can be eliminated by the M1 cells at a rate d_u (since high numbers of infiltrating M1 macrophages are associated with good patient prognosis (Mantovani, Schioppa, Porta, Allavena, & Sica, 2006). However, the presence of M2 cells inhibits the anti-tumour immune response generated by these M1 cells (Sica et al., 2008). Moreover, these M2 cells support tumour growth through the cytokines they secrete (Allavena & Mantovani, 2012).
- The virus-infected tumour cells die at a rate δ_i, following viral replication and cell burst – see also Equation (1c). The infected cells can be detected and eliminated (through phagocytosis) by the M1 macrophages (Hashimoto, Moki, Takizawa, Shiratsuchi, & Nakanishi, 2007; Italiani & Boraschi, 2014). The anti-viral effect of M1 cells is inhibited by the presence of M2 cells.

- Virus injection is described by function $H(t)$ (usually a pulse-like function; see the beginning of Section 3 below). The number of viral particles increases following the burst of infected tumour cells. We denote by b the burst size (i.e. the number of viral particles released by one infected cell). The half-life of these viral particles is $1/\omega$. Moreover, the M1 macrophages can promote an anti-viral immune response, which leads to early clearance of virus particles at a rate δ_v (Denton et al., 2016). This viral clearance can be suppressed by the M2 macrophages (Denton et al., 2016).
- The M1 macrophages are activated, at a rate a_1^v, by viral pathogens and infected tumour cells that trigger the secretion of pro-inflammatory cytokines (such as IFN-γ) (Labonte,Tosello-Trampont, & Hahn, 2014). These macrophages could also be activated, at a small rate a_1^u, by uninfected tumour cells (if they detect these tumour cells). The macrophages proliferate logistically at a rate p_{m1}, up to their carrying capacity M (note that tissue-resident macrophages proliferate via a self-renewal process rather than through an influx of progenitors (Italiani & Boraschi, 2014). The re-polarization of M1→M2 macrophages occurs (i) at a constant rate r_{m1}^0 (due to cytokines, such as IL-4, IL-10, TGF-β, which can be produced by different types of healthy and immune cells), and (ii) at a tumour-dependent rate $r_{m1}^u x_u/(h_u + x_u)$ (due to the anti-inflammatory cytokines produced by the tumour cells, e.g. TGB-β). The re-polarization of M2→M1 macrophages occurs at a constant rate r_{m2}^0 (due to cytokines such as IFN-γ or IL-12 produced by different types of cells in the environment). We note here that some viruses (e.g. SARS-CoV (Labonte et al., 2014), or paramyxoviruses (Tan et al., 2016)) do benefit from triggering a M2→M1 re-polarization. Moreover, oncolytic viruses can be engineered to carry chemokines and cytokines that can induce a macrophages polarization towards the M1-phenotype (Guiducci et al., 2005). We assume that this M2→M1 re-polarization occurs at a rate r_{m2}^v. Finally, the macrophages (M1 and M2) have a half-life of $1/d_e$.
- The M2 macrophages are activated at a rate a_2^u by cytokines such as IL-4, IL-10, IL-13, TGF-β, which are usually associated with a tumour-promoting environment (Labonte et al., 2014). These macrophages proliferate logistically at a rate p_{m2}, up to their carrying capacity M. The M2↔M1 re-polarization has been discussed in the previous paragraph.

2.1. Parameter approximation

Before investigating the dynamics of system (1), we first need to approximate the values of the parameters. In the following we discuss the approaches taken to identify (i) the parameter values associated with tumour dynamics alone, (ii) the parameter values for the tumour–immune interactions and (iii) the parameter values associated with the virus dynamics. These values are summarized in Table A2 (Appendix 1).

(i) *Tumour dynamics alone.* We first note that B16 melanoma cells have a doubling time between 17.2 and 24 h (Danciu et al., 2013; Calvet, André, & Mir, 2014). This corresponds to a proliferation rate of $r \in \left(\frac{\ln(2)}{(24/24)}, \frac{\ln(2)}{(17.2/24)}\right) = (.69, .97)$/day. For the simulations we use an average value of $r = .924$ corresponding to a doubling time of 18 h. For the tumour carrying capacity K we focus on the data in Chen et al. (2011),

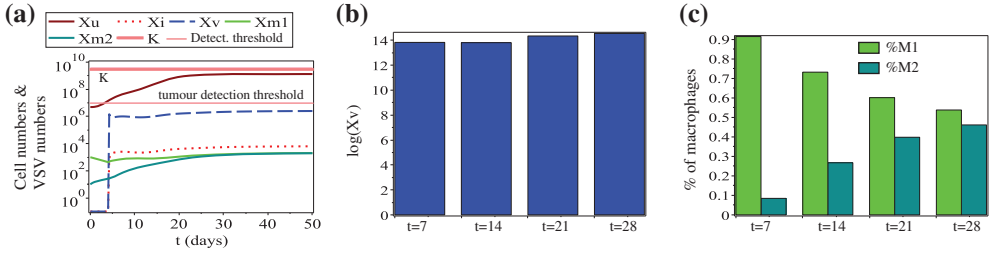

Figure 5. Dynamics of model (1) for the baseline parameter values listed in Table A2, and for the initial conditions listed in Table A1. Sub-panel (a) shows the tumour–immune–virus dynamics. Sub-panel (b) shows log ($x_v(t)$) at four specific days: $t = 7$, $t = 14$, $t = 21$ and $t = 28$. Sub-panel (c) shows the percentages of M1 and M2 macrophages in the system, at four specific days: $t = 7$, $t = 14$, $t = 21$ and $t = 28$.

Notes: The two horizontal upper lines describe the tumour detection threshold of $\approx 10^7$ cells/vol (see Friberg & Mattson, 1997) and tumour carrying capacity $K = 3.3 \times 10^9$.

where the maximum recorded tumour volume in the absence of any treatment was 3300 mm^3. Assuming that a volume of 1000 mm^3 contains approximately 10^9 tumour cells (Friberg & Mattson, 1997), we obtain a carrying capacity $K = 3.3 \times 10^9$ cells.

(ii) *Immune response.* It is known that during steady-state conditions, circulating monocytes have a half-life of 1–3 days (Yang, Zhang, Yu, Yang, & Wang, 2014), with some class of murine monocytes (Ly6C$^-$) exhibiting a longer steady-state half-life of 5–7 days (Italiani & Boraschi, 2014). Moreover, this half-life can be increased by certain drugs. For example, Ly6C$^-$ monocytes in tamoxifen-treated mice can show a half-life of up to 11 days (Yona et al., 2013). Finally, we need to mention that some macrophage populations can persist even longer, with macrophages residing in intestinal lamina propria having a half-life of three weeks, and alveolar macrophages persisting for years (Yona et al., 2013). For the simulations we consider an average cell death rate of $d_e = .2$/day (corresponding to a half-life of 3.4 days). In regard to the macrophages carrying capacity, we take the approach in Eftimie and Hamam (2017) and assume that $M = 10^8$.

To approximate the rest of parameters associated with the anti-tumour immune response, we use a least-squares approach to fit model (1) with no VSV ($x_v = x_i = 0$) to the mean of the tumour data, as well as to the levels of M1 and M2 cells on days 7 and 14, as given in Chen et al. (2011) (see also Figure 2(a) and (a')). Note that it makes sense to assume that following the injection of 5×10^6 tumour cells into C57BL/6 mice there is an innate immune response; moreover a recorded tumour doubling time of 18 h for B16F10 cells (Calvet et al., 2014; Danciu et al., 2013), cannot explain the slow tumour growth in Chen et al. (2011) – see also Figure 2(a). In Figure 4(a)–(a") we graph: (a) the time evolution of tumour–immune cells, (a') a comparison between numerical tumour growth and tumour data from Chen et al. (2011), and (a") a comparison between the numerics and the data for the percentages of M1 and M2 macrophages in the system at two different days: $t = 7$ and $t = 14$. The tumour and immune parameter values (d_u, h_u^m, h_m, d_m, a_1^u, a_2^u, p_{m1}, p_{m2}, r_{m1}^0, r_{m2}^0, r_{m1}^u) that generated these results are listed in Table A2. We note that due to the large size of

the parameter space, it is possible to obtain also other sets of parameter values that fit the data in Chen et al. (2011). However, it is not the purpose of this particular study to identify all these parameter values (especially since these values depend on the initial conditions of the experimental system and of the mathematical model, as well as the linear/non-linear interaction terms used in model (1)); rather we focus on one set of parameter values and investigate the dynamics of the model when we incorporate the VSV therapy.

We note that to be able to explain the M1:M2 ratios on days 7 and 14, as well as the slightly higher M1 percentages observed in Chen et al. (2011) on day 7, compared to the M2 percentages on day 14, we need to have $a_1^u < a_2^u$. Moreover, the M1→M2 re-polarization rate as a result of tumour growth (r_{m1}^u) needs to be much larger than the baseline re-polarization rates (r_{m1}^0 and r_{m2}^0). All these differences between parameters are captured in Table A2.

(iii) *Virus dynamics.* The burst size of the VSV varies between 50 plaque-forming units per cell (PFU/cell) to 8000 PFU/cell, with an average of 2500 PFU/cell (Zhu, Yongky, & Yin, 2009). Here, we run most of the simulations with baseline parameter $b = 2500$. Moreover, cells infected with VSV particles are lysed by the virus particles within 30-40 h post infection (Zhu et al., 2009). We assume an average of 35 h, and thus, consider $\delta_i = \ln(2.0)/35\,\text{h} = .47/\text{day}$. Regarding the intracellular half-life of VSV particles, it has been shown by DePolo and Holland (1986) that it can vary between 5.3 and 12.5 h, depending on the viral mutant. Moreover, the extracellular half-life of retroviral vectors pseudotyped with VSV-G glycoprotein is between 3.5 and 8 h (Hwang and Schaffer, 2013). In this study we assume a VSV half-life of 8 h, which corresponds to a viral death rate $\omega = \ln(2.0)/(8/24)/\text{day} = 2.0/\text{day}$. Finally, to approximate the rest of the parameters associated with the VSV interactions with tumour and immune cells, we fit the full model (1) to the mean of B16F10 tumour growth data following VSV infection, as re-drawn from Fernandez et al. (2002); see also Figure 4(b)–(b'). The parameter values (a_1^v, d_v, $d_i = \delta_v$, h_u) that generated these results are listed in Table A2. Again, we need to emphasize that the large parameter space (including the various choices for the length of the VSV injection time as described by the function $H(t)$) and the variety of initial conditions for the model variables, allows for different sets of parameter values to fit the tumour data in Fernandez et al. (2002).

3. Results

Since the majority of experimental studies in the literature focus on tumour–immune dynamics in the few days/weeks after the administration of the oncolytic virus, we start our investigation of model (1) by focusing on the transient behaviour of this system, as we vary different model parameters associated with the viral and immune responses. To this end, we model the experimental case where $\approx 5 \times 10^6$ tumour cells are injected into the system. Five days later (when the tumour has grown above a detection threshold of about 10^7 cells (Friberg & Mattson, 1997)), 10^7 VSV particles are injected into the tumour. Since the injection of VSV particles is usually performed within a couple of minutes/hours, and the virus starts being eliminated from the system within minutes after the injection

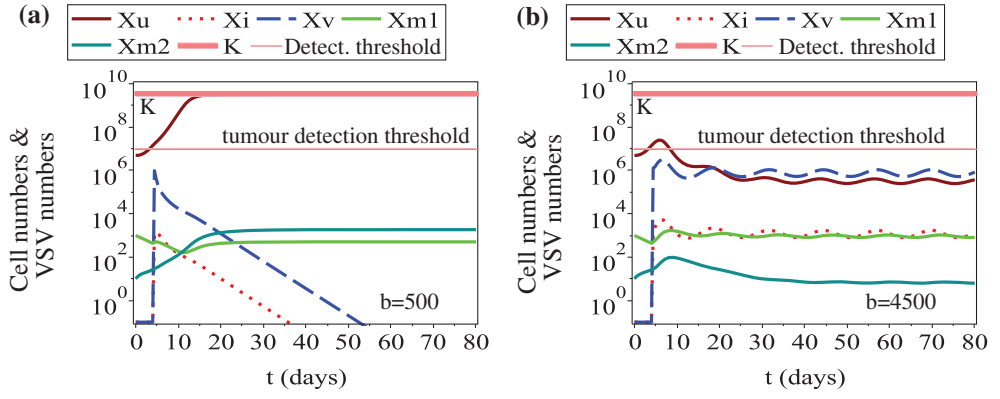

Figure 6. Dynamics of system (1) as we vary the VSV burst size: (a) $b = 500$, (b) $b = 4500$. The lower horizontal thick line describes the tumour detection threshold, which according to Friberg and Mattson (1997) is of at least 10^7 cells, while the upper horizontal line describes the carrying capacity K.

(Kubo et al., 2011; Pecora et al., 2002; Tesfay et al., 2013), we decided to represent this short injection time with the help of function $H(t) = \text{Heaviside}(5.2 - t) \cdot \text{Heaviside}(t - 5.1)$ (which is non-zero for 10% of a day, and zero for the rest of the time). Finally, we assume that when the tumour is injected, the circulating M1 macrophages – which are the primary host response (Mills & Ley, 2014) – discover within minutes some tumour-associated antigens (Arnold, Gordon, Baker, & Wilson, 2015). These assumptions translate into the initial conditions for the numerical simulations that are described in Table A1, Appendix 1 (i.e. approximately 10^3/vol M1 macrophages and approximately 10^0/vol M2 macrophages). Note that we have performed simulations also with zero initial levels of macrophages (not shown here), and the long-term results are qualitatively similar to the ones shown throughout the rest of this study.

Starting with these initial conditions, to propagate the solution in time we are using the predictor–corrector Adams–Bashforth–Moulton method, where the initial steps are calculated with the help of the fourth-order Runge–Kutta method. For the simulations, we use a time step of 10^{-3} (corresponding to minutes, and thus, accounting for the possible steep changes in the system dynamics that can occur within minutes/hours). In Figures 5–8, the solutions are shown as they evolve across days.

3.1. Short-term dynamics

We start our numerical investigation into the dynamics on model (1) by showing in Figure 5 the baseline behaviour of this model in the presence of VSV therapy (i.e. dynamics obtained with the initial conditions listed in Table A1 and the parameter values listed in Table A2; see Appendix 1). In this case the tumour grows to its carrying capacity K, despite the presence of some virus particles and tumour-infiltrating macrophages (with M1>M2 at least up to $t = 28$). For long-term model dynamics see Appendix 2.

In the following we investigate numerically the effects of changing various parameters on the transient dynamics of the tumour–immune–virus system. For now, we assume that $r^v_{m2} = 0$ (i.e. the oncolytic virus is not engineered to induce a M2→M1 re-polarization).

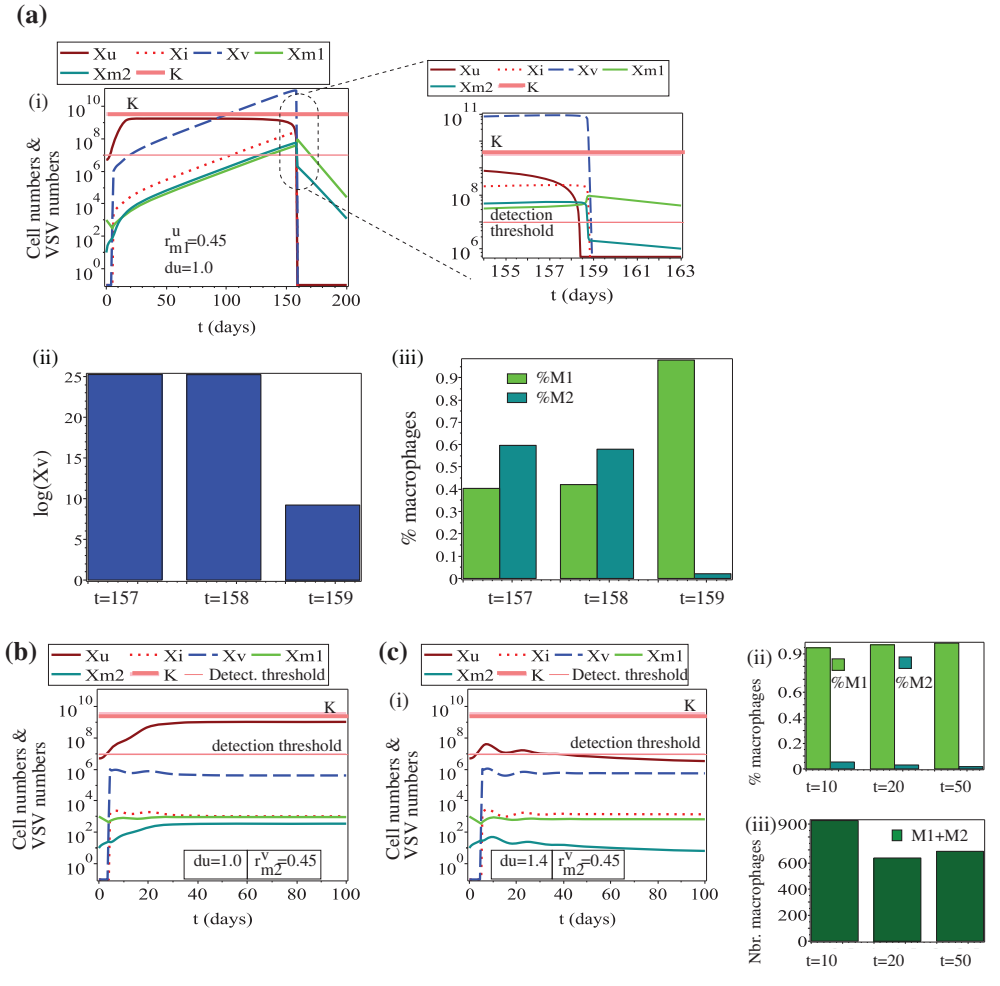

Figure 7. (a) The effect of increasing the re-polarization rate r^u_{m1} from the baseline value of .15 to $r^u_{m1} = .45$. Sub-panels (i) show the dynamics of tumour cells, immune cells and virus particles. Sub-panels (ii) show the logarithm of the level of VSV particles ($\ln(x_v)$) in three different days around the tumour elimination time: $t = 157$, $t = 158$ and $t = 159$. Sub-panels (iii) show the percentages of M1 and M2 cells in the system at the three different days. (b) The effect of increasing the re-polarization rate r^v_{m2} from the baseline value of 0 to $r^v_{m2} = .45$. (c) The effect of increasing the re-polarization rate r^v_{m2} to $r^v_{m2} = .45$, and the tumour-elimination rate d_u to $d_u = 1.4$ (in response to tumour-associated antigens on VSV). Sub-panels (ii) and (iii) show the percentages of M1 and M2 cells, and total numbers of M1+M2 cells at three different days: $t = 10$, $t = 20$, $t = 50$.

3.1.1. The effect of different VSV burst sizes

Since the VSV-infected cells could produce between 50 and 8000 progeny virus particles (Zhu et al., 2009) (with virus production depending on cell-to-cell differences), next we investigate the effect of changing parameter b within the range $b \in [500, 4500]$

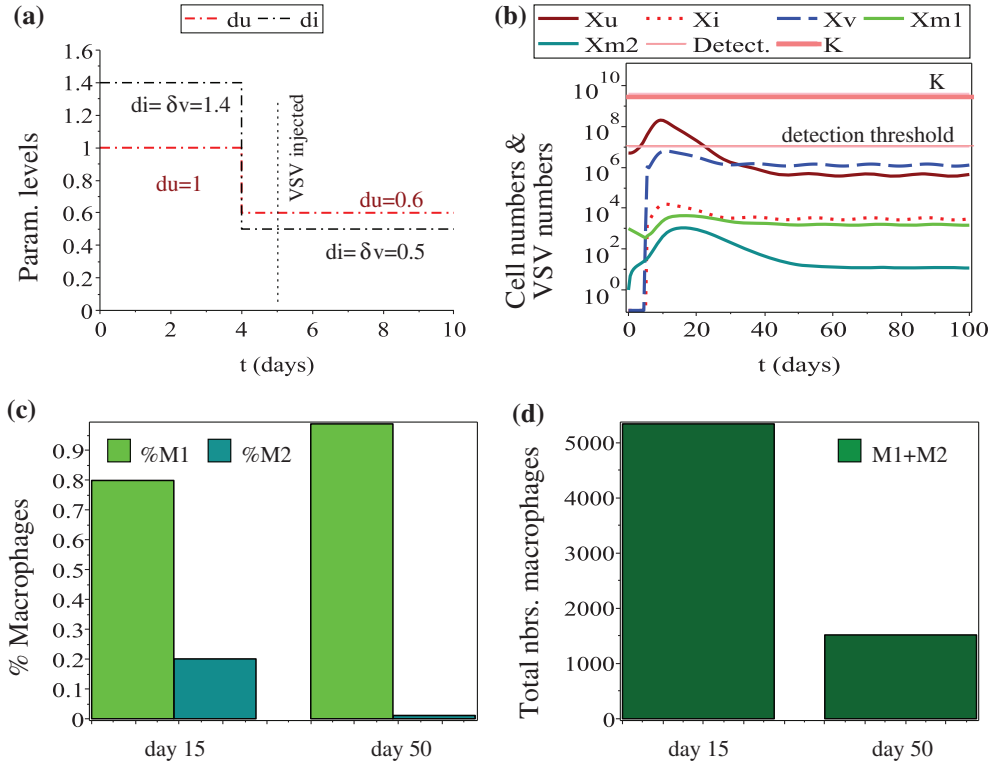

Figure 8. Dynamics of model (1) as we reduce, for *longer term*, the parameters d_u, d_i, δ_v that control the M1 (anti-tumour and anti-viral) immune response. (a) Reduction in parameter values on day $t = 4$, before the VSV is injected. (b) Time evolution of tumour cells, immune cells and virus particles. (c) Percentages of M1 and M2 macrophages on day 15 (when the tumour starts to be reduced) and on day 50 (when the tumour is being kept under control). (d) Total number of macrophages on days 15 and 50.

(as we fix all other parameters at their baseline level – see Table A2). In Figure 6(a) we observe that for very low values of b, the oncolytic virus is eliminated (and the system approaches a virus-free state, with the tumour cells at their carrying capacity). As we increase parameter b past the threshold value $b \approx 4300$, the system exhibits oscillations in the dynamics of the tumour, virus and immune responses (see Figure 6(b)). However, these oscillations occur after the tumour decreases below the detection threshold of $\approx 10^7$ cells (Friberg & Mattson, 1997), and thus, the tumour cannot be observed clinically.

3.1.2. The effect of increasing r^u_{m1} and r^v_{m2}

The generally accepted idea is that a re-polarization of M2 macrophages towards the M1 phenotype could improve the outcome of the therapy (Colombo & Mantovani, 2005; Zheng et al., 2017). Moreover, since viral infections that take place early in life are usually associated with a higher rate of viral replication due to M2 macrophage polarization (Sang, Miller, & Blecha, 2015), it raises the question of whether a (temporary) maintenance of the M2 phenotype following viral infection to enhance initial oncolytic viral titres could

improve the overall anti-tumour response. In the following we investigate: (a) the effect of increasing the M1→M2 re-polarization rate r^u_{m1} and (b) the effect of increasing the M2→M1 re-polarization rate r^v_{m2} (e.g. by genetically engineering the virus). Figure 7(a) shows that the increase in r^u_{m1} from $r^u_{m1} = .15$ (baseline value) to $r^u_{m1} = .45$ (panels (a)) leads to tumour elimination as a result of increased viral replication inside the large tumour. This oncolytic anti-tumour response triggers also a sharp increase in the M1:M2 ratio (and the total number of macrophages), which eventually contributes to the final elimination of the tumour. Note that while the tumour is very large, it is still slightly below its carrying capacity.

We have also investigated the effect of increasing the M2→M1 re-polarization rate as a result of using VSV particles engineered to carry chemokines and cytokines that can induce a macrophages polarization towards the M1-phenotype (Guiducci et al., 2005). (Previous studies have shown that VSV engineered to carry cytokines, such as IL-4, lead to enhanced anti-tumour activity; see Fernandez et al. (2002).) Figure 7(b) shows the effect of increasing r^v_{m2} from $r^v_{m2} = 0$ (baseline) to $r^v_{m2} = .45$ (we choose a rate greater than $r^u_{m1} = .15$ to ensure a strong polarization towards the M1 phenotype). Although this increase in r^v_{m2} leads to a large M1:M2 ratio, the low rate (d_u) at which the M1 cells eliminate the tumour cells does not cause a significant reduction in tumour size. In Figure 7(c), we then tested the assumption that the oncolytic virus also carries a tumour-associated antigen (as done experimentally in Bridle et al. (2009)), and thus, starting with day 5, when the VSV is introduced, the tumour-elimination rate d_u increases to the values of d_i and δ_v (the viral elimination rates): $d_u = 1.4$. This leads to a decrease in tumour size below the clinical detection threshold of $\approx 10^7$ (Friberg & Mattson, 1997). Here, tumour reduction is mainly the result of the anti-tumour immune response (i.e. a very large M1:M2 ratio – see sub-panel (ii)), and not so much of the oncolytic viral response).

Remark 1: Since other mathematical modelling studies discussed the importance of baseline re-polarization rates on tumour growth/decay (den Breems & Eftimie, 2016; Eftimie & Hamam, 2017), we also investigate this aspect. However, we observed that neither the increase in r^0_{m1} (from .001 to .1) nor the increase in r^0_{m2} (from .01 to .1) had any significant effect on tumour and viral dynamics, which was similar to the baseline dynamics shown in Figure 5. The only small difference was observed when we increased r^0_{m1} to .1, which lead to a ratio M2:M1> 1 during tumour relapse on for $t \geq 21$; in contrast to the case of M2:M1<1 for $t = 21, 28$ shown in Figure 5(c).

3.1.3. The effect of reducing the M1 immune response

Because the innate immune response is responsible for the persistence or elimination of the virus (Alvarez-Breckenridge, Yu, Kaur, Caligiuri, & Chiocca, 2012), next we investigate the effect of reducing (at the same time) the rate at which the M1 cells can eliminate the uninfected tumour cells (d_u), infected tumour cells (d_i) and viruses (δ_v). To this end, we investigate both (A) the long-term reduction in the immune response, and (B) the short-term reduction in the immune response. Since in the Discussion section we will emphasize the contradictory experimental results related to the role of M1/M2 cells vs. the M1+M2 tumour-infiltrating macrophages, next we pay particular attention to both percentages of M1/M2 cells and the total number (M1+M2) of macrophages.

(A) *Long-term reduction.* We assume that the immune response is reduced (via external chemical treatment; see Hesketh et al., 2015; Wehner et al., 2007; Zheng et al., 2017) on day $t = 4$, before the VSV is injected into the system (at $t = 5$). Figure 8(a) shows the levels of parameters that are reduced. Figure 8(b) shows that a reduction in the overall immune response leads to tumour decrease below the detection threshold of 10^7 cells (Friberg & Mattson, 1997). Therefore, although the tumour is not completely eliminated, it cannot be detected clinically, being kept under control by both the virus and the innate immune response. Note here that a very large ratio of M1:M2 cells (for example, $x_{m1}(50) \approx 99\%$ and $x_{m2}(50) \approx .1\%$) does not lead to tumour elimination, suggesting that the numbers of tumour-infiltrating macrophages are also very important on the overall outcome.

(B) *Short-term reduction.* It is known that VSV induces acute lymphopenia characterized by a reduction in the $CD8^+$ T cells for 2–4 days following virus injection. However, we do not have any knowledge of a similar phenomenon in macrophages. In consequence, we investigate at a theoretical level the effect of temporarily reducing the immune response between day $t = 5$ (when VSV is injected) and days $t = 8$ or $t = 30$ (the latter day assumes that a longer-time immune reduction is achieved via additional administration of external chemical molecules which can inhibit macrophages function; see Wehner et al. (2007) and Hesketh et al. (2015) or induce macrophages apoptosis (Zheng et al., 2017)). We note in Figures 9(ii) the reduction in tumour size associated with both an increase in VSV and a large M1:M2 ratio. In regard to long-term survival we remark that the M1:M2 ratio is larger than 70:30 (see sub-panels (iii)). This seems to be consistent with experimental data in Ohri et al. (2009), which showed that long-time patient survival is associated with more than 70% M1 islet macrophages and less than 30% M2 islet macrophages. Moreover, we note in panels (iv) that tumour reduction can be associated with both low and high numbers of macrophages (see total macrophages on day $t = 15$). In fact, in panel (a), tumour reduction is associated with a higher M1:M2 ratio, while in panel (b) tumour elimination is associated with a larger number of macrophages (M1+M2) combined with a higher M1:M2 ratio. Similarly, tumour growth can be associated with both low and high numbers of macrophages (see total macrophages on day $t = 50$). However, in this case M1:M2≈ 1; see panel (b)(ii) for $t > 60$.

Overall, the results presented in Figures 5–9 show that model (1) can exhibit a large variety of unintuitive behaviours, which depend on a variety of combinations of parameters. These unintuitive behaviours are the result of the feedback interactions between the VSV particles, macrophages and tumour cells. In Section 3.2, we explore a bit more the effect of these feedback interactions in the context of a local sensitivity analysis.

3.2. Tumour and VSV sensitivity to parameters

Since many model parameters were estimated, in the following we perform a local sensitivity analysis to investigate the changes in the uninfected tumour size, as we change the baseline parameters in Table A2. Because we are interested in identifying the parameters that can slow down tumour relapse, we focus on changes in tumour size (and VSV level) on day $t = 20$, when the tumour usually grows towards its carrying

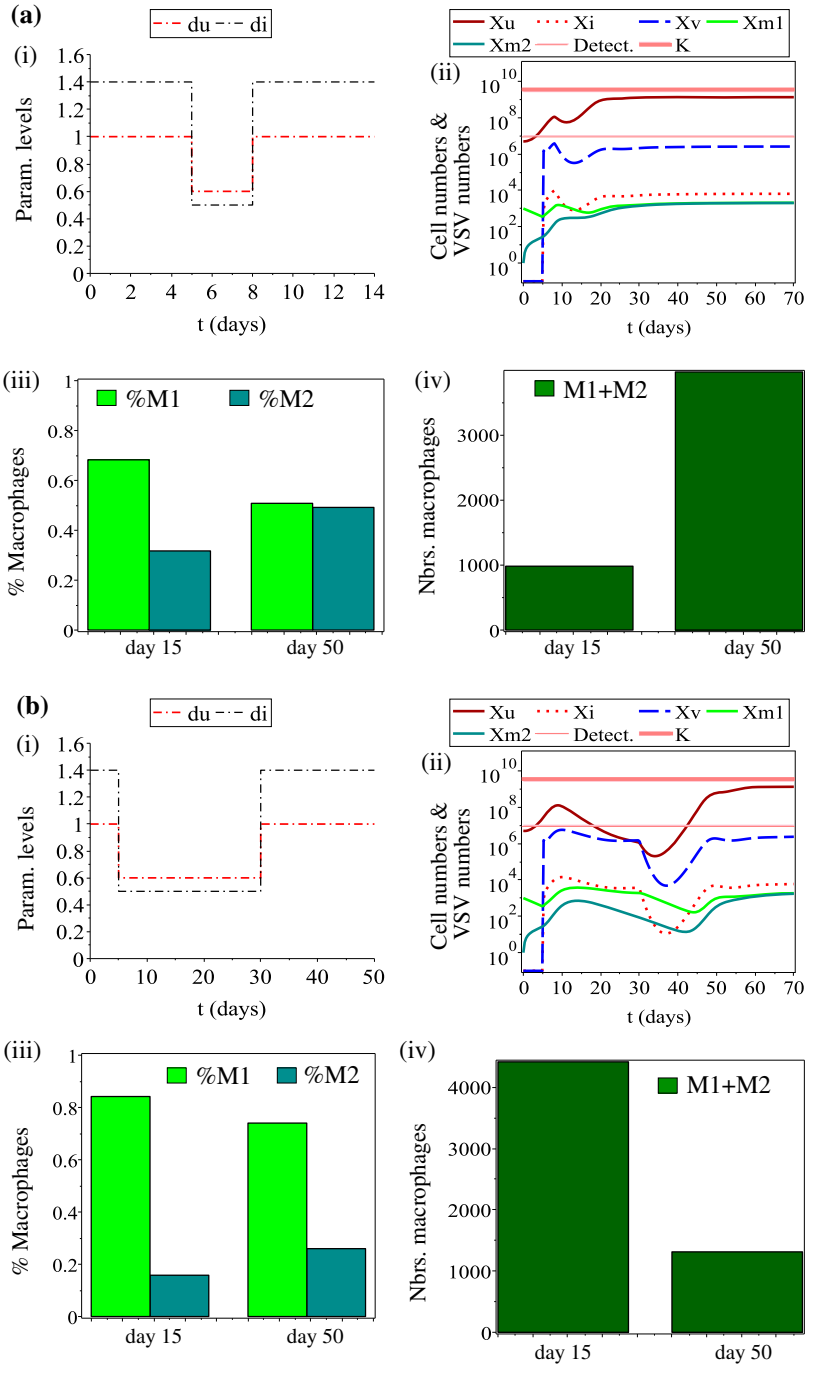

Figure 9. Dynamics of model (1) as we reduce, for *short-term*, the parameters d_u, d_i, δ_v that control the M1 (anti-tumour and anti-viral) immune response. (a) Reduction in parameter values between days $t = 5$ and $t = 8$. (b) Reduction in parameter values between days $t = 5$ and $t = 30$. Panels (i) show the level of reduced parameters. Panels (ii) show the time evolution of tumour cells, immune cells and virus particles. Panels (iii) show the percentages of M1 and M2 macrophages on day 15 (when the tumour is being reduced) and on day 50 (when the tumour is being kept under control). Panels (iv) show the total number of macrophages on days 15 and 50.

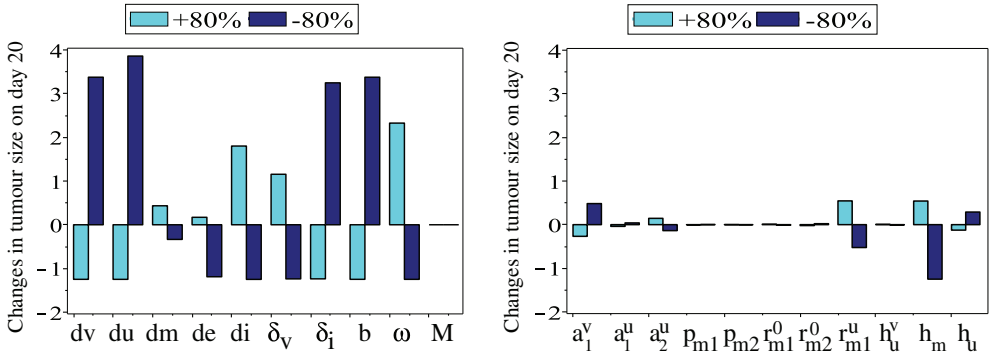

Figure 10. Relative sensitivity of tumour size on day $t = 20$, to $\pm 80\%$ changes in the baseline parameter values listed in Table A2.

Notes: Note that we did not include the tumour sensitivity to parameter r^v_{m2}, since the baseline value of this parameter is 0. Neither did we include tumour sensitivity to tumour growth rate (r) and carrying capacity (K) – since it is expected that the tumour size is very sensitive to changes in these two parameters (Eftimie et al., 2010).

capacity – see Figure 4(b'). Figures 10 and 11 show the relative changes in $x_u(20)$ and $x_v(20)$ as calculated by the formula (Hamby, 1994; Olufsen & Ottesen, 2013): $\frac{\Delta x_{u,v}}{x_{u,v}} / \left|\frac{\Delta \text{param}}{\text{param}}\right| = \frac{x^{old}_{u,v}(20) - x^{new}_{u,v}(20)}{x^{old}_{u,v}(20)} / \left|\frac{\text{param}^{old} - \text{param}^{new}}{\text{param}^{old}}\right|$, where $\text{param}^{new} = \text{param}^{old} \pm 80\% \text{param}^{old}$, and $\Delta x_{u,v}$ and Δparam are the finite difference approximations of the derivatives of $x_{u,v}$ and of *param*. Note that we chose to vary the initial parameter values by $\pm 80\%$ since we aim to explore large parameter fluctuations – especially important since we do not know the biologically realistic ranges for many of the parameter values (e.g. d_u, d_m, h^v_u, h_m, a^v_1, a^u_1, a^u_2; see Table A2).

In Figure 10, we remark the large impact that parameters d_v, d_u d_e, d_i, δ_v, δ_i, b, ω, h_m and r^u_{m1} have on decreasing tumour size on day 20 (thus, slowing down tumour relapse). Here, we ignored the tumour-related parameters r and K (since it is known that they will cause large changes in tumour size; see Eftimie, Bramson, & Earn, 2010), and focused only on immune and virus-related parameters. While some parameters (e.g. d_u, b, ω, r^u_{m1}) are expected to have a significant impact on tumour growth/decay, the effect of other parameters (e.g. d_e, h_m – associated with immune responses) was somehow unexpected. Particularly surprising is that a decrease in the natural elimination rate of macrophages d_e (i.e. an increase in the half-life of both M1 and M2 cells) could lead to a significant reduction in tumour size (just above the tumour detection level: $x^{new}_u(20) \approx 3.9 \times 10^7$; not shown here). This suggests that large numbers of macrophages (both M1 and M2) inside the tumour microenvironment could keep the tumour under control in the context of oncolytic virotherapies. This is an unexpected result since in the absence of the virus, large numbers of tumour-associated macrophages have been shown to correlate with decreased melanoma patient survival (Jensen et al., 2009; Makitie, Summanen, Tarkkanen, & Kivela, 2001).

To get a better understanding of the interactions between the injected VSV particles and the tumour-immune system during the transient period when the tumour relapses (i.e. before $t = 25$ days), we perform also a sensitivity of VSV on day $t = 20$ to the changes (by $\pm 80\%$) in model parameters. Figure 11 shows the relative changes in the

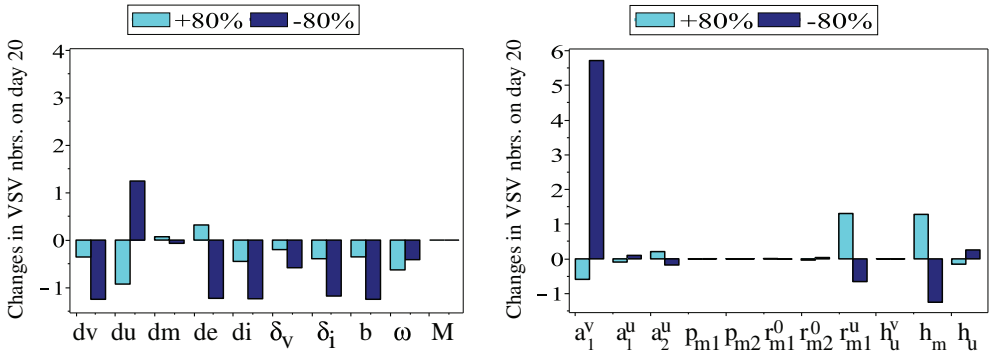

Figure 11. Relative sensitivity of VSV on day $t = 20$, to changes by $\pm 80\%$ in the baseline parameter values listed in Table A2.
Notes: Note that we focused mainly on sensitivity to immune-related and virus-related parameters, and thus, we ignored parameters r and K. Further, we ignored parameter r^v_{m2}, since its baseline value is 0.

sensitivity coefficient for VSV particles (where, as before, we ignored the tumour-related parameters r and K). The most important result is related to the non-linear effects that many parameters have on the VSV level: increasing as well as decreasing d_v, d_i, δ_v, δ_i, b, ω leads to a reduction in the VSV level on day $t = 20$. Moreover, it is unexpected that parameters such as ω or δ_i that enter Equations (1c) and (1b) in a linear fashion, have such a non-linear effect on the overall VSV dynamics. This is likely the effect of the feedback between VSV, M1/M2 macrophages and tumour cells. In this context, we also note that the parameter with the largest impact on VSV level is a^v_1, the rate at which VSV particles and virus-infected tumour cells activate the M1 macrophages (which then eliminate the VSV particles). Moreover, increasing/decreasing a^v_1 by 80% affects VSV with different intensities: a decrease in a^v_1 leads to a bigger change in VSV level compared to an increase in a^v_1. Overall, these sensitivity results suggest that individual-level variations in the parameters associated with the immune responses could have unexpected effects on the persistence of oncolytic viruses and their anti-tumour roles during transient tumour dynamics.

4. Discussion

In this paper, we considered a mathematical modelling and computational approach to investigate the complex interactions between an oncolytic virus (VSV) and the innate immune response generated by the M1 and M2 macrophages, which can be found inside solid tumours. While it is recognized that macrophages play a critical role in the anti-tumour immune response and the anti-viral immune response, their role on oncolytic viral therapies is a poorly understood aspect. Moreover, since various experimental studies emphasized the role of M1:M2 ratio as a tumour prognostic factor (Chen et al., 2011; He et al., 2013; Herwig, Bergstrom, Wells, Höller, & Grossniklaus, 2013; Zhang et al., 2011), we also paid particular attention to the percentages of M1 and M2 cells in the system, and their interactions with the VSV particles. In addition, since other studies suggested that it is not the M1/M2 ratio itself but the densities of

tumour-infiltrating macrophages that could predict long-term survival (Edin et al., 2012), we also calculated the total number of macrophages in the system for some cases where the tumour was eliminated, kept under control by the immune response, or grew to very large sizes.

We showed that changes in the tumour-induced re-polarization rate r_{m1}^{u} and the virus-induced re-polarization rate r_{m2}^{v} can lead to tumour elimination or reduction to very low sizes (see Figure 7). In this case, tumour elimination is the result of oncolytic therapy (see Figure 7(a)), while tumour reduction and control at very low sizes is the result of very high M1:M2 ratios – but not large numbers of tumour-infiltrating macrophages (see Figure 7(c)). Additional simulations (not shown here) concluded that changes in the baseline M1↔M2 re-polarization rates r_{m1}^{0}, r_{m2}^{0} do not affect significantly tumour dynamics, but they might affect the M1:M2 ratios that characterize tumour relapse (see Remark 1). This was slightly different from the simulations in den Breems and Eftimie (2016) and Eftimie and Hamam (2017), and was likely the result of the very low baseline values for r_{m1}^{0}, r_{m2}^{0} (which were obtained by fitting model (1) to data in Chen et al. (2011)).

In regard to the controversy related to the importance of large M1:M2 ratios vs. large/small numbers of tumour-infiltrating macrophages on long-term patient survival (Edin et al., 2012; He et al., 2013; Ohri et al., 2009), our numerical results showed that in the context of VSV oncolytic therapy, in some cases the M1:M2 ratio is important (see Figure 6(c), 7(c), 8 and 9(a)), while in other cases the total number of tumour-infiltrating macrophages (M1+M2) is important (see Figure 9(b)), and the results depend on various interaction rates and on the level of VSV infection. Therefore, the complexity of the tumour microenvironment allows for various treatment outcomes, and thus, we might not be able to use separately either the M1:M2 ratio or the number of M1 and M2 cells infiltrating the tumour as prognostic factors for long-term patient survival. However, combining both these factors could allow us to make predictions on long-term survival. Moreover, the importance of both numbers and percentages of M1 and M2 cells could have some impact on the current approaches used to deal with tumour-infiltrating macrophages in the context of improving cancer therapies (i.e. inhibition of macrophages recruitment into the tumours, induction of macrophages apoptosis, or re-polarization of M2 macrophages towards an M1-like phenotype; see Zheng et al., 2017).

Since in Chen et al. (2011) the authors showed only the percentages of M1 and M2 macrophages, we could not test the model against experimental data on total macrophages levels. (This emphasizes the necessity of having detailed experimental data to be able to make accurate quantitative and qualitative predictions on treatment outcomes.) However, we note that for the numerical simulations to reproduce the experimental results in Chen et al. (2011), higher levels of active macrophages would require much lower tumour-killing and tumour-promoting rates (d_u and d_m). Therefore, the values of d_u and d_m listed in Table A2 could be seen as upper threshold values for these two rates.

In regard to the interactions between the oncolytic virus (VSV) and macrophages, we note that higher virus levels ($\approx 10^{11}$PFU/vol) could lead to an increase in the macrophages population (both M1 and M2 cells; see Figure 7(a)), since the M1 macrophages are assumed to respond to foreign pathogens (and M1 cells then re-polarize into M2 cells). Moreover, long-term investigation of the dynamics of system (1) showed that higher VSV levels could

lead to (I) tumour elimination (see Figures 7 and B3(c)-in Appendix 2), or (II) tumour persistence associated with larger tumours and more M2 cells; see Figure B3(c) in Appendix 2. This dual elimination/persistence result, which is an outcome of the complex feedback interactions between the components of the system, could explain the contradictory results on tumour treatments in the literature (both in terms of M1:M2 ratios and numbers (He et al., 2013; Ohri et al., 2009), and in terms of the friend/foe roles that macrophages have on oncolytic viruses in the context of different tumours (Denton et al., 2016)). The importance of the complex feedback interactions between the oncolytic virus and the immune innate response on overall model dynamics became clear in the sensitivity analysis, where we observed the non-linear effect that changes in some interaction rates has on the level of VSV particles on day $t = 10$ (see Figure 11).

Finally, we acknowledge that the macrophages interact with other immune cells in the microenvironment (e.g. $CD8^+$ T cells, $CD4^+$ T cells, NK cells), which also have a role in tumour elimination. The purpose of this study was not to investigate all these possible immune interactions, but rather to focus on the pro-tumour and anti-tumour effects of M2 and M1 macrophages and their effects on the oncolytic virus therapy. The interactions between the macrophages and other immune cells (e.g. $CD8^+$ T cells) are the subject of a future study.

Disclosure statement

No potential conflict of interest was reported by the authors.

ORCID

R. Eftimie http://orcid.org/0000-0002-9726-1498

References

Allavena, P., & Mantovani, A. (2012). Immunology in the clinic review series; focus on cancer: Tumour-associated macrophages: Undisputed stars of the inflammatory tumour microenvironment. *Clinical and Experimental Immunology, 167*, 195–205.

Alvarez-Breckenridge, C. A., Yu, J., Kaur, B., Caligiuri, M. A., & Chiocca, E. A. (2012). Deciphering the multifaceted relationship between oncolytic viruses and Natural Killer cells. *Advances in Virology*, 702839.

Arnold, C. E., Gordon, P., Baker, R. N., & Wilson, H. M. (2015). The activation status of human machophages presenting antigen determines the efficiency of Th17 responses. *Immunobiology, 220*, 10–19.

Bajzer, Z., Carr, T., Josić, K., Russell, S. J., & Dingli, D. (2008). Modeling of cancer virotherapy with recombinant measles viruses. *Journal of Theoretical Biology, 252*, 109–122.

Bridle, B. W., Boudreau, J. E., Lichty, B. D., Brunellière, J., Stephenson, K., Koshy, S., ... Wan, Y. (2009). Vesicular stomatitis virus as a novel cancer vaccine vector to prime antitumor immunity amenable to rapid boosting with adenovirus. *Moleular Theory, 17*(10), 1814–1821.

Calvet, C. Y., André, F. M., & Mir, L. M. (2014). The culture of cancer cell lines as tumorspheres does not systematically result in cancer stem cell enrichment. *PLoS One, 9*(2), e89644.

Cassetta, L., Cassol, E., & Poli, G. (2011). Macrophage polarisation in health and disease. *TheScientificWorldJOURNAL, 11*, 2391–2402.

Chen, P., Huang, Y., Bong, R., Ding, Y., Song, N., Wang, X., ... Luo, Y. (2011). Tumour-associated macrophages promote angiogenesis and melanoma growth via adrenomedullin in a paracrine and autocrine manner. *Clinical Cancer Research, 17*(23), 7230–7239.

Colombo, M. P., & Mantovani, A. (2005). Targeting myelomonocytic cells to revert inflammation-dependent cancer promotion. *Cancer Research, 65*(20), 9113–9116.
Crivelli, J. J., Földes, J., Kim, P. S., & Wares, J. R. (2012). A mathematical model for cell cycle-specific cancer virotherapy. *Journal of Biological Dynamics, 6*, 104–120.
Danciu, C., Falamas, A., Dehelean, C., Soica, C., Radeke, H., Barbu-Tudoran, L., ... Munteanu, M. F. (2013). Characterisation of four B16 murine melanoma cell sublines molecular fingerprint and proliferative behaviour. *Cancer Cell International, 13*, 1–12.
den Breems, N., & Eftimie, R. (2016). The re-polarisation of M2 and M1 macrophages and its role on cancer outcomes. *Journal of Theoretical Biology, 390*, 23–39.
Denton, N. L., Chen, C.-Y., Scott, T. R., & Cripe, T. P. (2016). Tumour-associated macrophages in oncolytic virotherapy: Friend or foe? *Biomedicines, 4*, 13.
DePolo, N. J., & Holland, J. J. (1986). The intracellular half-lives of non-replicating nucleocapsids of DI particles of wild type and mutant strains of vesicular stomatitis virus. *Virology, 151*(2), 371–378.
Dingli, D., Offord, C., Myers, R., Peng, K.-W., Carr, T. W., Josic, K., ... Bajzer, Z. (2009). Dynamics of multiple myeloma tumor therapy with a recombinant measles virus. *Cancer Gene Therapy, 16*(12), 873–882.
Edin, S., Wikberg, M. L., Dahlin, A. M., Rutegard, J., Öberg, A., Oldenborg, P. A., & Palmqvist, R. (2012). The distribution of macrophages with a M1 or M2 phenotype in relation to prognosis and the molecular characteristics of colorectal cancer. *PLoS ONE, 7*(10), e47045.
Eftimie, R., Bramson, J. L., & Earn, D. J. D. (2010). Modeling anti-tumor Th1 and Th2 immunity in the rejection of melanoma. *Journal of Theoretical Biology, 265*(3), 467–480.
Eftimie, R., Dushoff, J., Bridle, B. W., Bramson, J. L., & Earn, D. J. D. (2011). Multi-stability and multi-instability phenomena in a mathematical model of tumor-immune-virus interactions. *Bulletin of Mathematical Biology, 73*(12), 2932–2961.
Eftimie, R., & Hamam, H. (2017). Modelling and investigation of the $CD4^+$ T cells - Macrophages paradox in melanoma immunotherapies. *Journal of Theoretical Biology, 420*, 82–104.
Eftimie, R., Macnamara, C., Dushoff, J., Bramson, J. L., & Earn, D. J. D. (2016). Bifurcations and chaotic dynamics in a tumour-immune-virus system. *The Mathematical Modelling of Natural Phenomena, 11*(5), 65–85.
Fernandez, M., Porosnicu, M., Markovic, D., & Barber, G. N. (2002). Genetically engineered vesicular stomatitis virus in gene therapy: Application for treatment of malignant disease. *Journal of Virology, 76*, 895–904.
Friberg, S., & Mattson, S. (1997). On the growth rates of human malignant tumoursL implications for medical decision making. *Journal of Surgical Oncology, 65*, 284–297.
Friedman, A., Tian, J. P., Fulci, G., Chiocca, E. A., & Wang, J. (2006). Glioma virotherapy: Effects of innate immune suppression and increased viral replication capacity. *Cancer Research, 66*(4), 2314–2319.
Goodridge, H. S., Ahmed, S. S., Curtis, N., Kollmann, T. R., Levy, O., Netea, M. G., ... Wilson, C. B. (2016). Harnessing the beneficial heterologous effects of vaccination. *Nature Reviews Immunology, 16*, 392–400.
Guiducci, C., Vicari, A. P., Sangaletti, S., Trinchieri, G., & Colombo, M. P. (2005). Redirecting in vivo elicited tumour infiltrating macrophages and dendritic cells towards tumour rejection. *Cancer Research, 65*, 3437–3446.
Guiot, C., Degiorgis, P., Delsanto, P., Gabriele, P., & Diesboeck, T. (2003). Does tumour growth follow a "universal law"? *Journal of Theoretical Biology, 225*, 147–151.
Hamby, D. M. (1994). A review of techniques for the parameter sensitivity analysis of the environmental models. *Environmental Monitoring and Assessment, 32*, 135–154.
Han, J., Chen, X., Chu, J., Xu, B., Meisen, W. H., Chen, L., ... You, J. (2015). TGFβ treatment enhances glioblastoma virotherapy by inhibiting the innate immune response. *Cancer Research, 75*(24), 5273–5282.
Hashimoto, Y., Moki, T., Takizawa, T., Shiratsuchi, A., & Nakanishi, Y. (2007). Evidence for phagocytosis of influenza virus-infected, apoptotic cells by neutrophils and macrophages in mice. *The Journal of Immunology, 178*(4), 2448–2457.

He, Y.-F., Zhang, M.-Y., Wu, X., Sun, X.-J., Xu, T., He, Q.-Z., & Di, W. (2013). High MUC2 expression in ovarian cancer is inversely associated with the M1/M2 ratio of tumour-associated macrophages and patient survival time. *PLoS ONE, 8*(12), e79769.

Herwig, M. C., Bergstrom, C., Wells, J. R., Höller, T., & Grossniklaus, H. E. (2013). M2/M1 ratio of tumour associated macrophages and PPAR-gamma expression in uveal melanomas with class 1 and class 2 molecular profiles. *Experimental Eye Research, 107*, 52–58.

Hesketh, A. J., Maloney, C., Behr, C. A., Edelman, M. C., Glick, R. D., Al-Abed, Y., ... Steiberg, B. M. (2015). The macrophage inhibitor CNI-1493 blocks metastasis in a mouse model of Ewing sarcoma through inhibition of extravasation. *PLoS ONE, 10*(12), e0145197.

Hofacre, A., Wodarz, D., Komarova, N. L., & Fan, H. (2012). Early infection and spread of a conditionally replicating adenovirus under conditions of plaque formation. *Virology, 423*(1), 89–96.

Hotte, S. J., Lorence, R. M., Hirte, H. W., Polawski, S. R., Bamat, M. K., O'Neil, J. D., ... Major, P. P. (2007). An optimized clinical regimen for the oncolytic virus PV701. *Clinical Cancer Research, 13*(3), 977–985.

Hwang, B.-Y., & Schaffer, D. V. (2013). Engineering a serum-resistant and thermostable vesicular stomatitis virus G glycoprotein for pseudotyping retroviral and lentiviral vectors. *Gene Therapy, 20*(8), 807–815.

Italiani, P., & Boraschi, D. (2014). From monocytes to M1/M2 macrophages: Phenotypical vs. functional differentiation. *Frontiers in Immunology, 5*, 514.

Jakeman, P. G., Hills, T. E., Fisher, K. D., & Seymour, L. W. (2015). Macrophages and their interactions with oncolytic viruses. *Current Opinion in Pharmacology, 24*, 23–29.

Jensen, T. O., Schmidt, H., Moller, H. J., Hoyer, M., Maniecki, M. B., Sjoegren, P., ... Steiniche, T. (2009). Macrophage markers in serum and tumour have prognostic impact in American Joint Committee on Cancer stage I/II melanoma. *Journal of Clinical Oncology, 27*(20), 3330–3337.

Kaufman, H. L., Kolhapp, F. J., & Zloza, A. (2016). Oncolytic viruses: A new class of immunotherapy drugs. *Nature Reviews, 14*, 642–662.

Kim, P. S., Crivelli, J. J., Choi, I.-K., Yun, C. O., & Wares, J. R. (2015). Quantitative impact of immunomodulation versus oncolysis with cytokine-expressing virus therapeutics. *Mathematical Biosciences and Engineering, 12*(4), 841–858.

Komarova, N. L., & Wodarz, D. (2010). ODE models for oncolytic virus dynamics. *Journal of Theoretical Biology, 263*(4), 530–543.

Kubo, T., Shimose, S., Matsuo, T., Fujimori, J., Sakaguchi, T., Yamaki, M., ... Ochi, M. (2011). Oncolytic vesicular stomatitis virus administered by isolated limb perfusion suppresses osteosarcoma growth. *Journal of Orthopaedic Research, 29*, 795–800.

Labonte, A. C., Tosello-Trampont, A.-C., & Hahn, Y. S. (2014). The role of macrophage polarization in infectious and inflammatory diseases. *Molecules and Cells, 37*(4), 275–285.

Laird, A. K. (1964). Dynamics of tumor growth. *The British Journal of Cancer, 18*, 490–502.

Liu, H., Yuan, S. J., Chen, Y. T., Xie, Y. B., Cui, L., Yang, W. Z., ... Tian, Y. T. (2013). Preclinical evaluation of herpes simplex virus armed with granulocyte-macrophage colony-stimulating factor in pancreatic carcinoma. *World Journal of Gastroenterology, 19*(31), 5138–5143.

Looney, W., Ritenour, E., & Hopkins, H. (1980). Changes in growth rate of an experimental solid tumour following increasing doses of cyclophosphamide. *Cancer Research, 40*, 2179–2183.

Louzoun, Y., Xue, C., Lesinski, G. B., & Friedman, A. (2014). A mathematical model for pancreatic cancer growth and treatments. *Journal of Theoretical Biology, 351*, 74–82.

Ma, J., Liu, L., Che, G., Yu, N., Dai, F., & You, Z. (2010). The M1 form of tumour-associated macrophages in non-small cell lung cancer is positively associated with survival time. *BMC Cancer, 10*, 112–120.

Macnamara, C., & Eftimie, R. (2015). Memory versus effector immune responses in oncolytic virotherapies. *Journal of Theoretical Biology, 377*, 1–9.

Makitie, T., Summanen, P., Tarkkanen, A., & Kivela, T. (2001). Tumour-infiltrating macrophages (CD68(+) cells) and prognosis in uveal melanoma. *Investigative Ophthalmology and Visual Science, 42*, 1414–1421.

Malinzi, J., Eladdadi, A., & Sibanda, P. (2017). Modelling the spatiotemporal dynamics of chemovirotherapy cancer treatment. *Journal of Biological Dynamics, 11*(1), 2244–2274.
Malinzi, J., Sibanda, P., & Mambili-Mamboundou, H. (2015). Analysis of virotherapy in solid tumour invasion. *Mathematical Biosciences, 263*, 102–110.
Mantovani, A., Schioppa, T., Porta, C., Allavena, P., & Sica, A. (2006). Role of tumour-associated macrophages in tumour progression and invasion. *Cancer and Metastasis Reviews, 25*(3), 315-322.
Mantovani, A., & Sica, A. (2010). Macrophages, innate immunity and cancer: Balance, tolerance, and diversity. *Current Opinion in Immunology, 22*, 231–237.
Mantovani, A., Sozzani, S., Locati, M., Allavena, P., & Sica, A. (2002). Macrophage polarization: Tumor-associated macrophages as a paradigm for polarized M2 mononuclear phagocytes. *TRENDS in Immunology, 23*(11), 549–555.
Meisen, W. H., Wohleb, E. S., Jaime-Ramirez, A. C., Bolyard, C., Yoo, J. Y., Russell, L., ... Kaur, B. (2015). The impact of macrophage and microglia secreted TNFα On oncolytic HSV-1 therapy in the glioblastoma tumor microenvironment. *Clinical Cancer Research, 21*(14), 3274–3285.
Melzer, M. K., Lopez-Martinez, A., & Altomonte, J. (2017). Oncolytic vesicular stomatitis virus as a viro-immunotherapy: Defeating cancer with a 'hammer' and 'anvil'. *Biomedicines, 5*(1), 8.
Mills, C., & Ley, K. (2014). M1 and M2 macrophages: The chicken and the egg of immunity. *The Journal of Innate Immunity, 6*(6), 716–726.
Nowak, M., & May, R. (2000). *Virus dynamics: Mathematical principles of immunology and virology*. Oxford, UK: Oxford University Press.
Ohri, C. M., Shikotra, A., Green, R. H., Waller, D. A., & Bradding, P. (2009). Macrophages within NSCLC tumour islets are predominantly of a cytotoxic M1 phenotype associated with extended survival. *The European Respiratory Journal, 33*, 118–126.
Olufsen, M. S., & Ottesen, J. T. (2013). A practical approach to parameter estimation applied to model predicting heart rate regulation. *Journal of Mathematical Biology, 67*(1), 39–68.
Paiva, L. R., Binny, C., Ferreira, S. C., Jr, & Martins, M. L. (2009). A multiscale mathematical model for oncolytic virotherapy. *Cancer Research, 69*(3), 1205–1211.
Pecora, A. L., Rizvi, N., Cohen, G. I., Meropol, N. J., Sterman, D., Marshall, J. L., ... Lorence, R. M. (2002). Phase I trial of intravenous administration of PV701, an oncolytic virus, in patients with advanced solid cancers. *Journal of Clinical Oncology, 20*(9), 2251–2266.
Rommelfanger, D. M., Offord, C. P., Dev, J., Bajzer, Z., Vile, R. G., & Dingli, D. (2012). Dynamics of melanoma tumour therapy with vesicular stomatitis virus: Explaining the variability in outcomes using mathematical modelling. *Gene Therapy, 19*(5), 543–549.
Sang, Y., Miller, L. C., & Blecha, F. (2015). Macrophage polarization in virus-host interactions. *Journal of Clinical and Cellular Immunology, 6*(2), 311.
Sica, A., Larghia, P., Mancino, A., Rubino, L., Porta, C., Totaro, M. G., ... Mantovani, A. (2008). Macrophage polarization in tumour progression. *Seminars in Cancer Biology, 18*, 349–355.
Tan, D. Q., Zhang, L., Ohaba, K., Ye, M., Ichiyama, K., & Yamamoto, N. (2016). Macrophage response to oncolytic paramyxoviruses potentiates virus-mediated tumour cell killing. *The European Journal of Immunology, 46*, 919–928.
Tesfay, M. Z., Kirk, A. C., Hadac, E. M., Griesmann, G. E., Federspiel, M. J., Barber, G. N., ... Russell, S. J. (2013). PEGylation of vesicular stomatitis virus extends virus persistence in blood circulation of passively immunized mice. *Journal of Virology, 87*(7), 3752–3759.
Wang, Y., Yang, T., Ma, Y., Halade, G., Zhang, J., Lindsey, M., & Jin, Y.-F. (2012). Mathematical modeling and stability analysis of macrophage activation in left ventricular remodeling post-myocardial infarction. *BMC Genomics, 13*, S21.
Wehner, S., Behrendt, F. F., Lyutenski, B. N., Lysson, M., Bauer, A. J., Hirner, A., & Kalff, J. C. (2007). Inhibition of macrophage function prevents intestinal inflammation and postoperative ileus in rodents. *Gut, 56*(2), 176–185.
Wodarz, D. (2001). Viruses as antitumor weapons: Defining conditions for tumor remission. *Cancer Research, 61*, 3501–3507.
Wodarz, D., & Komarova, N. (2009). Towards predictive computational models of oncolytic virus therapy: Basis for experimental validation and model selection. *PLOS One, 4*(1), e4271.

Wu, J. T., Kirn, D. H., & Wein, L. M. (2004). Analysis of a three-way race between tumor growth, a replication-competent virus and an immune response. *Bulletin of Mathematical Biology, 66*(4), 605–625.

Yang, J., Zhang, L., Yu, C., Yang, X.-F., & Wang, H. (2014). Monocyte and macrophages differentiation: Circulation inflammatory monocyte as biomarker for inflammatory diseases. *Biomarker Research, 2*, 1.

Yona, S., Kim, K.-W., Wolf, Y., Mildner, A., Varol, D., Breker, M., ... Jung, S. (2013). Fate mapping reveals origins and dynamics of monocytes and tissue macrophages under homeostasis. *Immunity, 38*(1), 79–91.

Yoshida, K., & Ishii, S. (2016). Innate immune memory via ATF-7-dependent epigenetic changes. *Cell Cycle, 15*(1), 3–4.

Yoshida, K., Maekawa, T., Zhu, Y., Renard-Guillet, C., Chatton, B., Inoue, K., ... Ishii, S. (2015). The transcription factor ATF7 mediates lipopolysaccharide-induced epigenetic changes in macrophages involved in innate immunological memory. *Nature Immunology, 16*(10), 1034–1043.

Zhang, B., Yao, G., Zhang, Y., Gao, J., Yang, B., Rao, Z., & Gao, J. (2011). M2-polarised tumour-associated macrophages are associated with poor prognoses resulting from accelerated lymphangiogenesis in lung adenocarcinoma. *Clinics, 66*(11), 1879–1886.

Zheng, X., Turkowski, K., Mora, J., Brüne, B., Seeger, W., Weigert, A., & Savai, R. (2017). Redirecting tumour-associated macrophages to become tumoricidal effectors as a novel strategy for cancer therapy. *Oncotarget, 8*(29), 48436–48452.

Zhu, Y., Yongky, A., & Yin, J. (2009). Growth of an RNA virus in single cells reveals a broad fitness distribution. *Virology, 385*(1), 39–46.

Appendix 1. Summary of model variables and parameters

Tables A1 and A2 summarize the variables (and their initial values) and the parameters that appear in system (1).

Table A1. Summary of initial conditions used for the numerical simulations of system (1).

Variable	Description	Initial conditions
x_u	Density of uninfected tumour cells (cell numbers per volume)	$x_u(0) = 5 \times 10^6$ (Chen et al., 2011)
x_i	Density of virus-infected tumour cells (cell numbers per volume)	$x_i(0) = 0$
x_v	Density of virus particles (described as particles forming units (PFU) per volume)	$x_v(0) = 0$
x_{m1}	Density of M1 macrophages (cell numbers per volume)	$x_{m1}(0) = 10^3$
x_{m2}	Density of M2 macrophages (cell numbers per volume)	$x_{m2}(0) = 1$

Table A2. Summary of model parameters and their values used throughout this study. The baseline parameter values used in the simulations are shown in parentheses, under the range values for the same parameters.

Param.	Value	Units	Description & references
r	.924	days^{-1}	Proliferation rate for tumour cells (Danciu et al., 2013)
K	3.3×10^9	cells/vol	Carrying capacity for the tumour cells Chen et al. (2011)
d_v	.0036	$(\text{cells/vol}) \times (\text{PFU/vol})^{-1} \times (\text{days})^{-1}$	Infection rate of tumour cells with the oncolytic virus
d_u	1.0	days^{-1}	Rate at which M1 macrophages eliminate uninfected tumour cells
d_m	.2	days^{-1}	Rate at which M2 macrophages support tumour growth
h_u^v	10^5	(cells/vol)	Half-saturation constant for the tumour cells infected with the oncolytic virus
h_m	10^3	(cells/vol)	Half-saturation constant for macrophages that support half the maximum immune response (leading to tumour elimination or tumour growth)
δ_i	.47	days^{-1}	Rate at which the oncolytic virus kills an infected tumour cell (Zhu et al., 2009)
d_i	1.4	days^{-1}	Rate at which the M1 macrophages eliminate the infected tumour cells
b	500-8000 (2500)	$(\text{PFU/vol}) \times (\text{cells})^{-1}(\text{vol})$	Number of virus particles released from an infected cell, capable of forming plaques (Zhu et al., 2009)
ω	2.0	days^{-1}	Death rate of oncolytic virus particles)
δ_v	1.4	$(\text{cells/vol}) \times (\text{PFU/vol})^{-1} \times (\text{days})^{-1}$	Rate at which the M1 macrophages eliminate the virus particles
a_1^v	2.4×10^{-4}	days^{-1}	Activation rate of M1 macrophages in response to viral antigens
a_1^u	5×10^{-8}	days^{-1}	Activation rate of M1 macrophages in response to viral antigens
a_2^u	1×10^{-7}	days^{-1}	Activation rate of M2 macrophages in response to tumour growth factors (TGF-β) or type-II cytokines in the tumour microenvironment
p_{m1}	10^{-3}	days^{-1}	Proliferation rate of M1 cells
p_{m2}	10^{-3}	days^{-1}	Proliferation rate of M2 cells
M	10^8	(cells/vol)	Carrying capacity of macrophages
r_{m1}^0	.0001–.1 (.001)	days^{-1}	Small baseline M1→M2 re-polarization rate in response to cytokines in the microenvironment (Wang et al., 2012; Eftimie and Hamam, 2017)
r_{m1}^u	.015–.45 (.15)	days^{-1}	M1→M2 re-polarization rate in response to tumour-supporting cytokines & growth factors
r_{m2}^0	.0001–.1 (.01)	days^{-1}	Small baseline M2→M1 re-polarization rate in response to cytokines in the microenvironment (Wang et al., 2012; Eftimie and Hamam, 2017)
r_{m2}^v	.0–.45 (0)	days^{-1}	M2→M1 re-polarization rate in response to engineered viruses
h_v	10	(PFU/vol)	Half-saturation constant for the viruses to trigger a M2→M1 re-polarization
h_u	10^8	(cells/vol)	Half-saturation constant for the tumour cells that can trigger an M1→M2 re-polarization
d_e	.2	days^{-1}	Natural death rate of macrophages (Yona et al., 2013)

Appendix 2. Long-term dynamics: steady-states

We have seen in Section 3.1 that in the long-term, the dynamics of the system (1) could approach either a fixed steady-state (see e.g. Figures 5 and 6(a)), or can exhibit a periodic behaviour (see Figure 6(c) and 8). In the following, we focus on identifying the possible steady-states exhibited by model (1), and their dependence on various model parameters. It can be easily shown that system (1) exhibits the following steady-states:

(i) Tumour-free, virus-free, macrophages-free state: $(x_u^*, x_i^*, x_v^*, x_{m1}^*, x_{m2}^*) = (0, 0, 0, 0, 0)$.

(ii) Tumour-free, virus-free, macrophages-present state: $(x_u^*, x_i^*, x_v^*, x_{m1}^*, x_{m2}^*) = (0, 0, 0, x_{m1}^*, x_{m2}^*)$, where x_{m1}^* and x_{m2}^* satisfy the following equation (where we made the assumption that the M1 and M2 macrophages have similar proliferation rates, $p_{m1} = p_{m2} := p_m$ – see Table A2):

$$\frac{r_{m1}^0}{r_{m2}^0} = \frac{1 + \frac{x_{m2}^*}{x_{m1}^*}}{1 + \frac{x_{m1}^*}{x_{m2}^*}} \tag{B1}$$

We graph in Figure B1(a) the changes in the ratio of x_{m1}^*/x_{m2}^* as a function of the ratio r_{m1}^0/r_{m2}^0. As expected, a larger M1:M2 ratio (i.e. M1>M2) corresponds to a lower baseline r_{m1}^0/r_{m2}^0 ratio.

(iii) Tumour-present, virus-free, macrophages-present state: $(x_u^*, x_i^*, x_v^*, x_{m1}^*, x_{m2}^*) = (x_u^*, 0, 0, x_{m1}^*, x_{m2}^*)$, with the non-zero variables given implicitly as follows:

$$x_u^* = K + \frac{K}{r}\frac{d_m x_{m2}^* - d_u x_{m1}^*}{h_m + x_{m2}^*}, \tag{B2a}$$

$$(a_2^u - a_1^u)x_u^* + 2x_{m1}^* r_{m1}^u \frac{x_u^*}{h_u + x_u^*} = x_{m2}^*(2r_{m2}^0 + d_e) - x_{m1}^*(2r_{m1}^0 + d_e). \tag{B2b}$$

We graph in Figure B1(b) the changes in the steady-state levels of M1 and M2 cells, as we vary the baseline re-polarization rates r_{m1}^0 and r_{m2}^0. Note that an increase in r_{m1}^0 leads to states with larger levels of x_{m2}^* cells and lower levels of x_{m1}^* cells (i.e. lower M1:M2 ratios). In contrast, an increase in r_{m2}^0 leads to states with lower levels of x_{m2}^* cells and higher levels of x_{m1}^* cells (i.e. higher M1:M2 ratios). Note that it is possible to have also steady-states with no M1 macrophages ($x_{m1}^* = 0$). The small figure on the right shows that for $x_{m1}^*, x_{m2}^* > 10^4$, there are new solution branches, characterized by $x_{m1}^* > x_{m2}^*$ (in the presence of tumours). The bottom figure shows the level of uninfected tumour cells x_u as a function of M1 and M2 macrophages. Note that small (or zero) tumours exist for ratios of $M1 : M2 > 1$, while large tumours exist for ratios of $M1 : M2 < 1$.

(iv) Tumour-present, virus-present, macrophages-present state: $(x_u^*, x_i^*, x_v^*, x_{m1}^*, x_{m2}^*)$, where the variables satisfy the following equations:

$$0 = r\left(1 - \frac{x_u^*}{K}\right) - \frac{d_v x_v^*}{h_u^v + x_u^*} - \frac{d_u x_{m1}^*}{h_m + x_{m2}^*} + \frac{d_m x_{m2}^*}{h_m + x_{m2}^*}, \tag{B3a}$$

$$x_i^* = \frac{d_v x_v^* x_u^*}{(h_u^v + x_u^*)\left(\delta_i + \frac{d_i x_{m1}^*}{h_m + x_{m2}^*}\right)}, \tag{B3b}$$

$$0 = \frac{d_v x_u^*}{(h_u^v + x_u^*)\left(\delta_i + \frac{d_i x_{m1}^*}{h_m + x_{m2}^*}\right)} - \frac{1}{\delta_i b}\left(\omega + \frac{\delta_v x_{m1}^*}{h_m + x_{m2}^*}\right), \tag{B3c}$$

$$0 = a_1^v(x_i^* + x_v^*) + x_u^*(a_1^u - a_2^u) - 2x_{m1}^*\left(r_{m1}^0 + r_{m1}^u \frac{x_u^*}{h_u + x_u^*}\right) + 2x_{m2}^*\left(r_{m2}^0 + r_{m2}^v \frac{x_v^*}{h_v + x_v^*}\right) - d_e x_{m1}^* + d_e x_{m2}^*. \tag{B3d}$$

We can simplify these equations if we solve Equation (B3a) for $x_{\rm v}^*$ and substitute it, together with Equation (B3b), into Equation (B3c). The solution is now given by the intersection of the following two surfaces in the $(x_{\rm m1}^*, x_{\rm m2}^*, x_{\rm u}^*)$ space:

$$S_1: \quad 0 = \frac{d_v x_{\rm u}^*}{(h_u^v + x_{\rm u}^*)\left(\delta_i + \frac{d_i x_{\rm m1}^*}{h_m + x_{\rm m2}^*}\right)} - \frac{1}{\delta_i b}\left(\omega + \frac{\delta_v x_{\rm m1}^*}{h_m + x_{\rm m2}^*}\right), \tag{B4a}$$

$$\begin{aligned} S_2: \quad 0 = {} & a_1^v\left[r\left(1 - \frac{x_{\rm u}^*}{K}\right) - \frac{d_u x_{\rm m1}^* - d_m x_{\rm m2}^*}{h_m + x_{\rm m2}^*}\right]\left[\frac{h_u^v + x_{\rm u}^*}{d_v} + \frac{x_{\rm u}^*}{\delta_i + \frac{d_i x_{\rm m1}^*}{h_m + x_{\rm m2}^*}}\right] \\ & + x_{\rm u}^*(a_1^u - a_2^u) - d_e(x_{\rm m1}^* - x_{\rm m2}^*) - 2x_{\rm m1}^*\left(r_{m1}^0 + r_{m1}^u \frac{x_{\rm u}^*}{h_u + x_{\rm u}^*}\right) \\ & + 2x_{\rm m2}^*\left\{r_{m2}^0 + \frac{r_{m2}^v\left(\frac{h_u^v + x_{\rm u}^*}{d_v}\right)\left[r\left(1 - \frac{x_{\rm u}^*}{K}\right) - \frac{d_u x_{\rm m1}^* - d_m x_{\rm m2}^*}{h_m + x_{\rm m2}^*}\right]}{h_v + \left(\frac{h_u^v + x_{\rm u}^*}{d_v}\right)\left[r\left(1 - \frac{x_{\rm u}^*}{K}\right) - \frac{d_u x_{\rm m1}^* - d_m x_{\rm m2}^*}{h_m + x_{\rm m2}^*}\right]}\right\}. \end{aligned} \tag{B4b}$$

We graph in Figure B2(a) the intersection curve between surfaces S_1 and S_2 as given by Equation (B4), for the baseline re-polarization rates $r_{m1}^0 = .001$ and $r_{m2}^0 = .01$. First note that these steady-states exist only for very large tumours (of more than 10^7 cells). An unexpected result (which explains also the long-term dynamics in Figures 6 and 8) is that the lower tumour states are characterized by a lower level of tumour-infiltrating macrophages, and if $x_{\rm m1}^* < 2 \times 10^3$ then $x_{\rm m1}^* < x_{\rm m2}^*$ (see the projection onto the $(x_{\rm m1}^*, x_{\rm m2}^*)$ plane in the right figure of panel (a)). In contrast, if $x_{\rm m1}^* > 2 \times 10^3$ then the state will have $x_{\rm m1}^* > x_{\rm m2}^*$. The low level of tumours is explained by high VSV values.

In Figure B2(b) we note that an increase in r_{m2}^0 leads to a slight increase of the x_u^* state, while an increase in r_{m1}^0 leads to a slight decrease in $x_{\rm u}^*$- see the small right figure in panel (b). Since $x_{\rm v}^*$ is incorporated into these intersection curves, this increase/decrease in $x_{\rm u}^*$ is the result of changes in $x_{\rm v}^*$ values, as shown below in Figure B3.

Figure B3 shows the relation between $x_{\rm u}^*$, $x_{\rm m1}^*$ and $x_{\rm m2}^*$ for four different $x_{\rm v}^*$ values. For low VSV values (panels (a),(b)), smaller tumours persist and are associated with $x_{\rm m1}^* > x_{\rm m2}^*$. Note here that larger tumours can also persist and are associated with either $x_{\rm m1}^* \geq x_{\rm m2}^*$ or $x_{\rm m1} \leq x_{\rm m2}^*$. This explains the numerical results in Figs. 6(b),(c), 8, 9. For higher VSV values (panels (c),(d)), only large tumours can exist (the smaller tumours being eliminated), and in this case $x_{\rm m2}^* \geq x_{\rm m1}^*$. The elimination of small and medium-sized tumours for $VSV \geq 10^{10}$ is consistent with the numerical simulations in Figure 7.

Since we are mainly interested in those cases where tumour is eliminated, in the following we focus only on the first two types of steady-states, (i) and (ii), and investigate their stability – to identify the biological and mathematical conditions for which system (1) can approach such steady-states.

- It can be easily shown that the tumour-free, virus-free, macrophages-free state (i) is always unstable (since the first eigenvalue of the Jacobian matrix associated with system (1) and calculated at the state $(0, 0, 0, 0, 0)$ is $\lambda_1 = r > 0$). Therefore, we do not expect this system to approach (for a very long time) a state where the tumour and the virus are eliminated and there is no persistent immune response. However, since this state is a saddle point, solution trajectories could approach this state along the stable manifold, and move away from the state along the unstable manifold.
- The stability of the tumour-free, virus-free, macrophages-present state (ii) depends on the model parameters, as the five eigenvalues of the Jacobian matrix associated with system (1) and calculated at the state $(0, 0, 0, x_{\rm m1}^*, x_{\rm m2}^*)$ are

$$\lambda_1 = -\frac{d_u x_{\rm m1}^* - d_m x_{\rm m2}^* - r x_{\rm m2}^* - r h_m}{h_m + x_{\rm m2}^*}, \tag{B5}$$

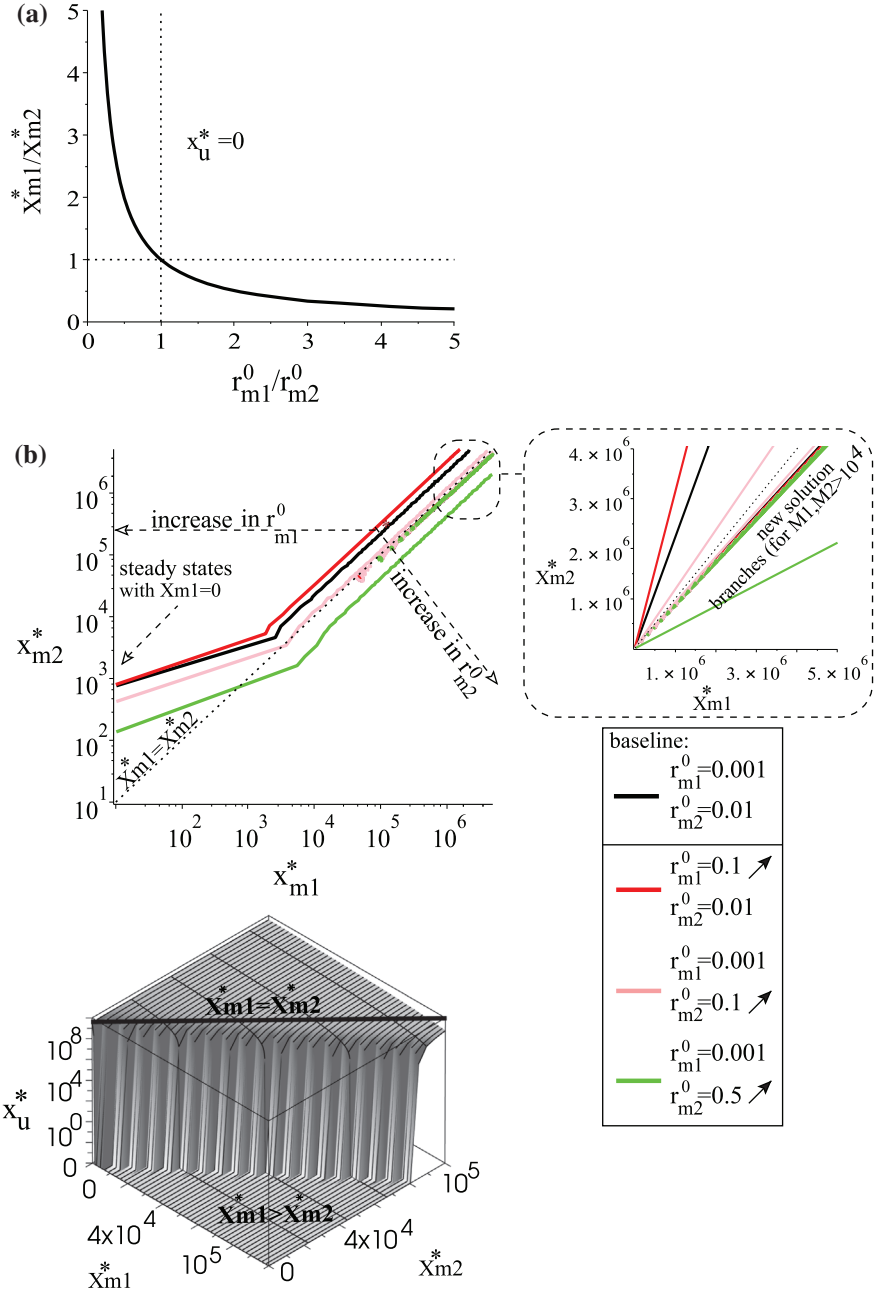

Figure B1. Virus-free steady-states. (a) Tumour-free, virus-free steady-state ($x_u^* = x_i^* = x_v^* = 0$): the ratio of x_{m1}/x_{m2} as a function of the baseline re-polarization ratio r_{m1}^0/r_{m2}^0; see also Equation (B1); (b) Tumour-present, virus-free, macrophages-present steady-state ($x_i^* = x_v^* = 0$): changes in x_{m1}^* and x_{m2}^*, as we vary the baseline re-polarization rates r_{m1}^0 and r_{m2}^0. Bottom figure shows x_u^* as a function of x_{m1}^* and x_{m2}^*.

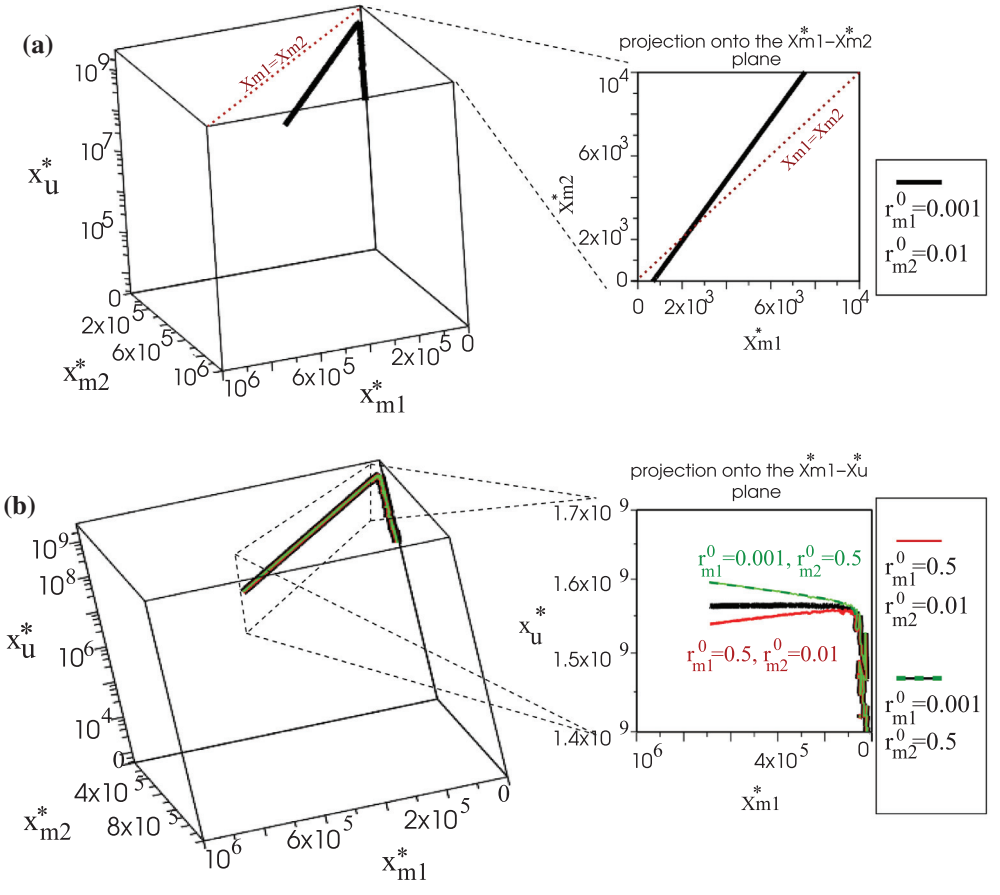

Figure B2. (a) Tumour-present, virus-present, macrophages-present steady-state: the curve represents the intersection of surfaces S_1 and S_2 given by Equations (B4a) and (B4b), for the baseline macrophages re-polarization rates $r^0_{m1} = .007$, $r^0_{m2} = .001$. (b) The intersection curve for surfaces S_1 and S_2 as we now vary the two baseline re-polarization rates: we increase r^0_{m1} to .5 while keeping $r_{m2} = .001$ fixed (red curve), and we increase r^0_{m2} to .5 while keeping $r_{m1} = .001$ fixed (green curve).
Note: These changes in r^0_{m1} and r^0_{m2} lead to changes in the tumour steady-state x^*_u.

$$\lambda_2 = -\frac{\delta_v x^*_{m1} + \omega x^*_{m2} + \omega h_m}{h_m + x^*_{m2}} \leq 0, \tag{B6}$$

$$\lambda_3 = -\frac{d_i x^*_{m1} + \delta_i x^*_{m2} + \delta_i h_m}{h_m + x^*_{m2}} \leq 0, \tag{B7}$$

and $\lambda_{4,5}$ satisfying the quadratic equation

$$\lambda^2 - \lambda(c_{11} + c_{22}) + c_{11}c_{22} - c_{12}c_{21} = 0, \tag{B8}$$

with

$$c_{11} = p_{m1}\left(1 - \frac{2x^*_{m1} + x^*_{m2}}{M}\right) - r^0_{m1} - d_e, \tag{B9}$$

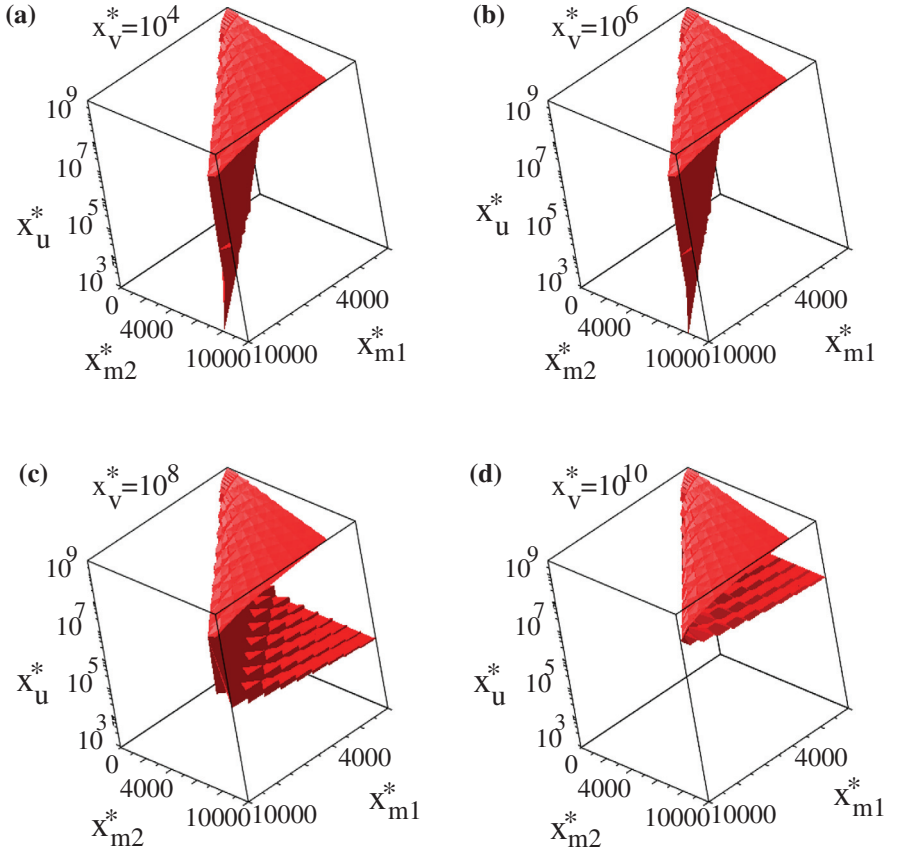

Figure B3. The relation between uninfected tumour cells (x_u^*), M1 (x_{m1}^*) and M2 (x_{m2}^*) cells, for four different levels of VSV, as described by Equation (B3a): (a) $x_v^* = 10^4$PFU/vol; (b) $x_v^* = 10^6$PFU/vol; (c) $x_v^* = 10^8$PFU/vol; (d) $x_v^* = 10^{10}$PFU/vol.

$$c_{12} = -\frac{p_{m1}x_{m1}^*}{M} + r_{m2}^0, \quad c_{21} = -\frac{p_{m2}x_{m2}^*}{M} + r_{m1}^0, \tag{B10}$$

$$c_{22} = p_{m2}\left(1 - \frac{x_{m1}^* + 2x_{m2}^*}{M}\right) - r_{m2}^0 - d_e. \tag{B11}$$

This tumour-free state is stable provided that $\lambda_1 \leq 0$ and $\lambda_{4,5} \leq 0$. The inequality $\lambda_1 \leq 0$ reduces to the following inequality for the ratio of M1 and M2 macrophages:

$$\frac{x_{m1}^*}{x_{m2}^*} \geq \frac{d_m + r}{du} + \frac{rh_m}{d_u x_{m2}^*}. \tag{B12}$$

This inequality could be satisfied if this ratio is greater than one. (Note also in Figure B1(b) bottom panel, that for $x_{m1}^* > x_{m2}^*$ it is possible to have states with no tumours.) The inequality $\lambda_{4,5} \leq 0$ reduces to $c_{11} + c_{22} \leq 0$ and $c_{11}c_{22} - c_{12}c_{21} \geq 0$, or equivalently (since $p_{m1} = p_{m2}$)

$$p_{m1}\left(1 - 3\frac{x_{m1}^* + x_{m2}^*}{M}\right) - 2d_e \leq r_{m1}^0 + r_{m2}^0, \tag{B13}$$

and

$$\left[p_{m1}\left(1-\frac{x^*_{\mathrm{m1}}+x^*_{\mathrm{m2}}}{M}\right)-d_e-(r^0_{m1}+r^0_{m2})\right]\left[p_{m1}\left(1-\frac{2(x^*_{\mathrm{m1}}+x^*_{\mathrm{m2}})}{M}\right)-d_e\right]\geq 0. \tag{B14}$$

For the parameter values used in this study (see also Table A2), inequality (B13) holds true since the term in the left-hand-side is negative (as $p_{m1} \ll d_e < 1$). For the same reason, also inequality (B14) holds true, as each of the two terms in the left-hand-side are negative for the parameter values used in this study; see also Table A2.

Therefore, for low baseline re-polarization ratios $r^0_{m1}/r^0_{m2} \leq 1$ we can obtain tumour-free states with high macrophages ratios $x^*_{\mathrm{m1}}/x^*_{\mathrm{m2}}$, and these states could be stable thus ensuring permanent tumour elimination. From a biological point of view, this tumour elimination requires the long-term persistence of M1 and M2 cells in the system, which might be possible due to recent research showing the existence of innate immune memory-like behaviours in macrophages (Goodridge et al., 2016; Yoshida & Ishii, 2016; Yoshida et al., 2015).